Key Points:
- Direct initialization of SM/ST is more effective than the sequential/indirect initialization in the ARW model
- Land conditions and evaporation control postlandfall rainfall, and land surface and rainfall coupling are sensitive to the former land state
- MD movement and postlandfall rainfall show significant improvement when the SM/ST conditions are initialized from LDAS products

Correspondence to:
K. K. Osuri,
osurik@nitrkl.ac.in;
osurikishore@gmail.com

Author Contributions:
Conceptualization: Krishna K. Osuri
Formal analysis: Krishna K. Osuri, Raghu Nadimpalli, Kumar Ankur, H. P. Nayak, A. K. Das, Dev Niyogi
Funding acquisition: Krishna K. Osuri, U. C. Mohanty, Dev Niyogi
Investigation: Krishna K. Osuri, Dev Niyogi
Methodology: Krishna K. Osuri, Raghu Nadimpalli, Kumar Ankur
Project administration: U. C. Mohanty, Dev Niyogi
Resources: U. C. Mohanty, A. K. Das, Dev Niyogi
Software: Kumar Ankur
Supervision: U. C. Mohanty, Dev Niyogi
Validation: Raghu Nadimpalli, Kumar Ankur, H. P. Nayak
(continued)

Improved Simulation of Monsoon Depressions and Heavy Rains From Direct and Indirect Initialization of Soil Moisture Over India

Krishna K. Osuri[1] , Raghu Nadimpalli[2] , Kumar Ankur[3] , H. P. Nayak[2], U. C. Mohanty[2] , A. K. Das[4], and Dev Niyogi[5,6]

[1]Department of Earth and Atmospheric Sciences, National Institute of Technology Rourkela, Rourkela, India, [2]School of Earth Ocean and Climate Sciences, Indian Institute of Technology Bhubaneswar, Bhubaneswar, India, [3]Department of Atmospheric and Earth Science, University of Alabama in Huntsville, Huntsville, AL, USA, [4]Numerical Weather Prediction Division, India Meteorological Division, New Delhi, India, [5]Department of Agronomy, Crops, Soils, and Water sciences, Department of Earth, Atmospheric, and Planetary Sciences, Purdue University, West Lafayette, IN, USA, [6]Department of Geological Sciences, Jackson School of Geosciences, Department of Civil, Architectural, and Environmental Engineering, University of Texas at Austin, Austin, TX, USA

Abstract This study investigates the impact of direct versus indirect initialization of soil moisture (SM) and soil temperature (ST) on monsoon depressions (MDs) and heavy rainfall simulations over India. SM/ST products obtained from high-resolution, land data assimilation system (LDAS) are used in the direct initialization of land surface conditions in the ARW modeling system. In the indirect method, the initial SM is sequentially adjusted through the flux-adjusting surface data assimilation system (FASDAS). These two approaches are compared with a control experiment (CNTL) involving climatological SM/ST conditions for eight MDs at 4-km horizontal resolution. The surface fields simulated by the LDAS run showed the highest agreement, followed by FASDAS for relatively dry June cases, but the error is high (~15–30%) for the relatively wet August cases. The moisture budget indicates that moisture convergence and local influence contributed more to rainfall. The surface-rainfall feedback analysis reveals that surface conditions and evaporation have a dominant impact on the rainfall simulation and these couplings are notable in LDAS runs. The contiguous rain area (CRA) method indicates better performance of LDAS for very heavy rainfall distribution, and the location (ETS > 0.2), compared to FASDAS and CNTL. The pattern error contributes the maximum to the total rainfall error, and the displacement error is more in August cases' rainfall than that in June cases. Overall analyses indicated that the role of land conditions is significantly high in the drier month (June) than a wet month (August), and direct initialization of SM/ST fields yielded improved MD and heavy rain simulations.

1. Introduction

During the southwest monsoon season, heavy to very heavy rainfall occurs over significant parts of India primarily due to organized mesoconvective systems such as monsoon depressions (MDs), lows, and midtropospheric circulations. Among these, MDs are considered responsible for nearly half to two thirds of the heavy rainfall events occurring over the Indian monsoon region (IMR) (Hunt & Fletcher, 2019; Sikka, 1978). Most of the MDs typically develop over the Bay of Bengal (BoB), close to land, and occasionally in the Arabian Sea (AS) before moving inland. As the MDs approach land, they interact with the underlying land surface and are influenced by features such as topography, as well as soil moisture (SM) and soil temperature (ST).

Prior studies report limited skill of mesoscale models for rainfall predictions from MDs (Bhowmik et al., 2007). The model performance has shown modest but promising improvements with the assimilation of atmospheric observations (Mohanty et al., 2012; Routray, Mohanty, Niyogi, et al., 2010; Routray, Mohanty, Rizvi, et al., 2010). Studies such as Niyogi et al. (2016), Hunt and Turner (2017), and Baisya et al. (2017) postulate that the limited improvements might be due to the unrealistic representation of land surface characteristics in the models. In the recent years, satellite-derived SM products such as from Soil Moisture Active Passive (SMAP), Soil Moisture and Ocean Salinity (SMOS), and European Space Agency-Climate Change Initiative (ESACCI) have become a useful source of spatiotemporally consistent data. These products are available on a subdaily basis. However, they have a relatively coarse spatial resolution

Visualization: Krishna K. Osuri, Raghu Nadimpalli, Kumar Ankur, H. P. Nayak

Writing - original draft: Krishna K. Osuri, Raghu Nadimpalli

Writing – review & editing: Krishna K. Osuri, Raghu Nadimpalli, Kumar Ankur, Dev Niyogi

(~10–25 km or more). The coarser resolution tends to smooth out the SM peak values that are particularly important for capturing the mesoscale boundaries and convection (Holt et al., 2006). As a result, these products need to be downscaled to capture the realistic heterogeneity in the SM conditions. A recent study demonstrated the marginal improvements from the assimilation of ESACCI SM in a land-surface data assimilation system over the Indian monsoon domain (Mohanty et al., 2019). Therefore, this study primarily focuses on the initialization of land surface conditions (SM and ST) prepared off-line at a high spatiotemporal resolution, to improve the prediction of MD simulation and heavy rainfall using the Advanced Research Weather Research and Forecasting (ARW) model.

The interaction between the land surface and atmosphere is considered essential and needs to be understood in the context of cumulus convective rainfall simulations (Osuri et al., 2017). The heterogeneity in land surface characteristics such as terrain, moisture, vegetation, and soil type over the IMR contributes to the heat and moisture feedback strongly influencing the regional weather, and hydroclimate applications including crop water management at field (Jamshidi et al., 2020). The warm, tropical region has noticeable diurnal changes in heat and moisture exchanges between the land and atmosphere, which ultimately modifies heat and moisture fluxes (Pielke, 2001), and evapotranspiration estimates (Jamshidi Zand-Parsa, Naghdyzadegan Jahromi, et al., 2019, Jamshidi, Zand-Parsa, Pakparvar, et al., 2019, Jamshidi et al., 2020), within the planetary boundary layer (PBL) and associated cumulus cloud activity (Taylor et al., 2011; Tuttle & Salvucci, 2016). Initial studies suggest that land surface heterogeneity and feedback could be influential on the convective structure of rain-bearing systems (Holt et al., 2006; Niyogi et al., 2006; Trier et al., 2004). Studies continue to demonstrate the value of accurate representation of land surface conditions for simulation of heavy rainfall events over the IMR (Chang, Kumar, et al., 2009; Chang, Niyogi, et al., 2009; Kishtawal et al., 2010; Lei et al., 2008; Nayak et al., 2018; Osuri et al., 2017). Indeed, several studies (e.g., Koster et al., 2004) demonstrate that the IMR is one of the prominent land-atmosphere coupling "hot spot" globally and that SM, in particular, can significantly influence the precipitation. SM continues to be one of the critical variables that need to be initialized in numerical weather prediction (NWP) models (Drusch, 2007; Mahfouf, 2010). Chang, Kumar, et al. (2009), building on earlier work of Dastoor and Krishnamurti (1991), showed a possible relation between antecedent SM representation—the so-called Brown Ocean Effect—in the ARW model and the postlandfall evolution of MDs. A number of related studies have been reported, such as Andersen et al. (2013), Andersen and Shepherd (2014), Bozeman et al. (2012), Kellner et al. (2012), and Kishtawal et al. (2013), and, recently, Nair et al. (2019) highlighted the influence of LC and SM on extreme rainfall cases from both tropical cyclones as well as MDs.

In this study, we assess two methods to update SM/ST initial conditions with the ARW modeling system. In the first method, realistic SM/ST conditions are directly initialized into the model from a land data assimilation system (LDAS). In another method, the surface conditions are adjusted through the flux-adjusting surface data assimilation system (FASDAS; Alapaty et al., 2008). Currently, SM/ST observations are not readily available over the IMR at high spatiotemporal scale to use in the direct method. Therefore, off-line-prepared SM/ST fields from the high-resolution land data assimilation system (HRLDAS; Chen et al., 2007, hereafter LDAS) based on the Noah land surface model (LSM) is used. These gridded, SM/ST data products are considered high quality and good surrogates for in situ, dense, SM/ST observational network (Nayak et al., 2018; Osuri et al., 2017). The ARW model Version 3.9.1 is used to study the simulation of eight MDs, and the impact on rainfall using the direct and indirect SM/ST initialization is investigated. The broader objective is to improve the mesoscale simulation of MDs and associated rain and to assess the impact of enhanced land surface conditions.

2. Methodology

There exists an emerging need for coupling land assimilation systems in the atmospheric models to improve heavy rainfall prediction over the IMR (Niyogi, 2019). As mentioned, both direct and indirect land data initialization methods have been adopted in this study. Eight MD cases that occurred from 2007 to 2013 are simulated. The details, such as the case name, the initial date of integration, and forecast length, are given in Table 1. A control run (CNTL) is carried out with initial and boundary conditions from the FiNaL analyses (FNL) of the National Centers for Environmental Prediction (NCEP) in 6-hr intervals. It is the default surface forcing that is adopted in most of the operational/research modeling activity over this region (Osuri

Table 1
Details on Model Initialization Time and Forecast Length of MD Cases

Cases	Initialization time of monsoon depression	Forecast length (hours)
1	2007-06-21_00	60
2	2007-06-28_00	60
3	2007-08-05_00	72
4	2008-06-16_00	72
5	2008-08-09_00	72
6	2011-06-16_00	84
7	2013-06-14_00	54
8	2013-08-20_00	54

et al., 2017). In the direct method (experiment known as LDAS), the SM/ST of LDAS products are used as surface forcing to the ARW model. In the indirect method (hereafter called as FASDAS), the SM is adjusted through flux-adjusting surface observational nudging method. The size of the nested model domain (outer domain at 12 km horizontal grid distance and inner domain at 4 km) is displayed in Figure 1a. Note that the initialization of surface fields is conducted in the 4-km nested domain, and the information is shared through a two-way nesting configuration. The LDAS has been run for the Indian domain to develop off-line SM and ST fields. The inner-nest domain (in Figure 1a) covers most of the Indian domain for which the products were developed. The inner domain was thus sufficiently large to develop the regional analysis for MD simulations. Also, we did not have ready access to additional in situ data from other nations, which was another factor to consider in selecting the inner domain. The model uses the Mellor Yamada Janjic (MYJ) PBL scheme, Monin-Obukhov Janjic surface-layer option, RRTM longwave, Dudhia shortwave radiation, and WSM6 microphysics. Both the domain uses Betts-Miller-Janjic convection scheme, following Routray, Mohanty, Niyogi, et al. (2010) and Routray, Mohanty, Rizvi, et al. (2010).

The LDAS is an uncoupled Noah-based LSM used to prepare regional SM and ST fields at four soil layers (0–10, 10–40, 40–100, and 100–200 cm) (Chen et al., 1996; Ek et al., 2003). The LDAS integrates observed/analyzed near-surface atmospheric parameters (2-m temperature and specific humidity, 10-m winds, surface pressure, model elevation, rain rate, downward shortwave, and longwave radiation) along with the surface static fields such as land use and soil type, and monthly vegetation characteristics. The advantage of LDAS is that it uses the same grid as the ARW model, sharing the same Noah LSM and same geophysical parameters (land use, soil texture, terrain height, and time-varying vegetation fields) and reduces interpolation errors. In this study, the LDAS is integrated to prepare regional SM/ST profiles at 4-km grid spacing over the IMR. The LDAS uses atmospheric forcing from MERRA (Bosilovich et al., 2012), rain rate from TRMM-3B42v7, and initial land surface conditions from the Global Data Assimilation System (GDAS). The methodology on the atmospheric forcing fields is available in Osuri et al. (2017) and Nayak et al. (2018). The LDAS is initialized on 1 January 1999 and integrated up to 31 December 2015. The first-year (1999) data are left out for spin-up (Charusombat et al., 2012).

In the indirect land-state initialization technique, the surface observations are assimilated continuously to improve the surface and boundary layer simulation (Alapaty et al., 2001, 2008). For example, the surface temperature and moisture observations are first nudged in the model's initial values of the ARW model. Then the difference between observation and model-predicted surface temperature and moisture is translated to update the respective surface fluxes. The updated surface sensible is used in the ground temperature prognostic equation, and the latent heat flux adjustment is partitioned into several new evaporative flux adjustments. These adjustments are then applied in the prognostic equation of SM at each soil layer. Such adjustments through the prognostic equation affect the simulation of surface fluxes in subsequent times and thereby modify the atmospheric boundary layer development. This technique of surface flux adjustment is known as FASDAS, and the method is proven to improve atmospheric surface and boundary layer simulations (Alapaty et al., 2008). This methodology has also been applied for the IMR to improve the simulation of MDs and associated rainfall using the Fifth-Generation Penn State/NCAR Mesoscale Model (MM5) model (Vinodkumar et al., 2008, 2009). In the current study, the FASDAS technique is applied to update the SM and ST conditions using surface measurements (~2-m temperature and moisture and 10-m winds). The surface observations are nudged 24 hr before the initial analyses in 6-hr intervals.

3. Data Used

In this study, various in situ observations, satellite-derived, and global analyses are used. The distribution of in situ observations used to verify the regional SM/ST fields developed from LDAS is shown in Figure 1a. The details of analyses and in situ observations such as period, spatial and temporal resolution are shown in Table 2. Brief information is discussed below.
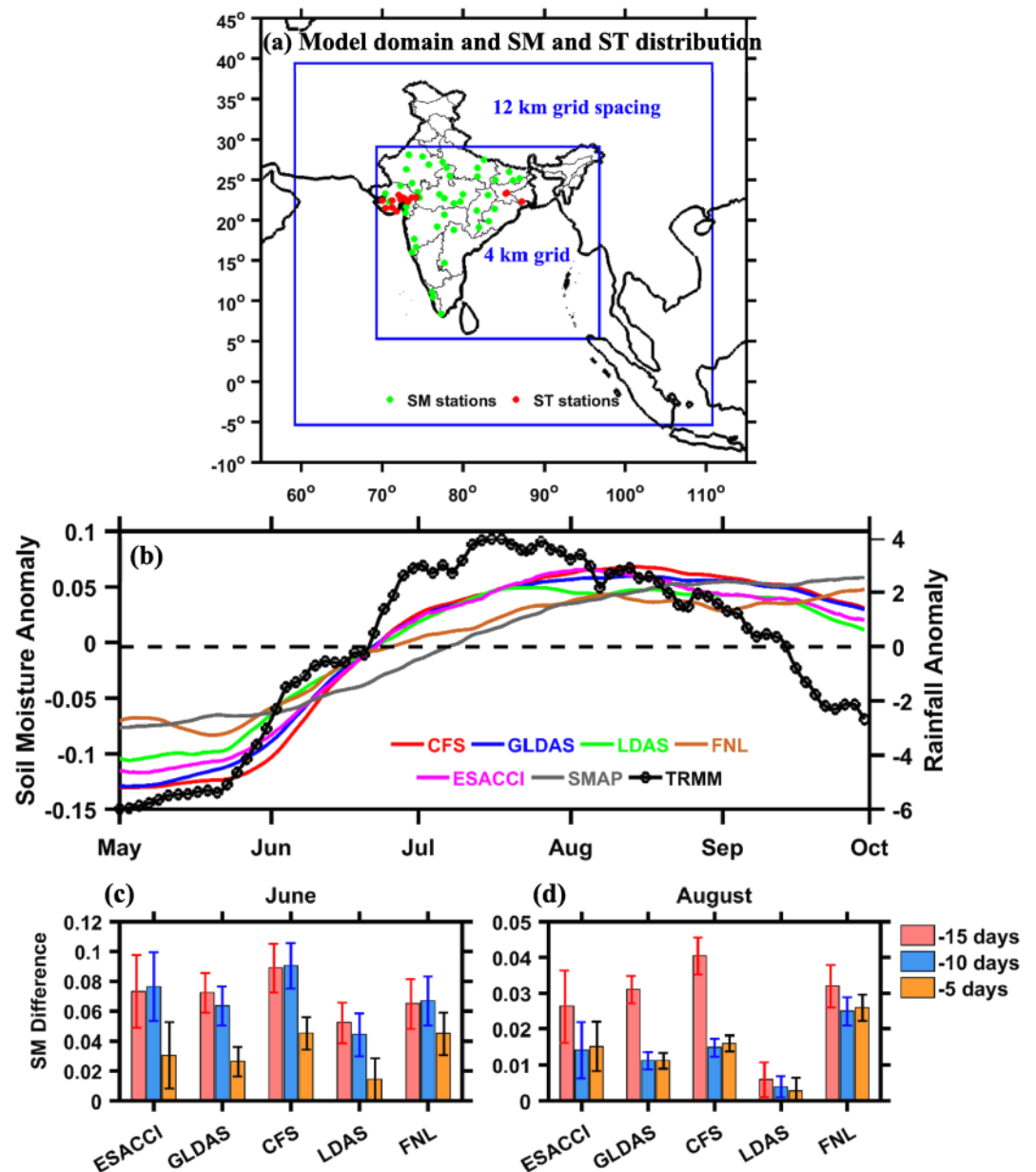
Figure 1. (a) Model domain configuration and distribution of SM and ST measurements. (b) The daily anomaly of SM (m^3 m^{-3}) obtained from various global and regional analyses (CFS, GLDAS, FNL, LDAS, ESACCI, and SMAP) along with daily anomaly of TRMM rainfall (mm day^{-1}) during May to September for central India. Mean SM difference between MD formation day and 15, 10, and 5 days before formation from various analyses for (b) June cases and (c) August cases along with 95% confidence intervals. The number of years considered in the climatology is shown in Table 1.

Top-layer SM in situ observations from 48 agromet automatic weather stations (AWSs) of India Meteorological Department (IMD) is obtained for the monsoon season (June – September) from CTCZ data bank (http://www.incois.gov.in/portal/datainfo/pdctcz.jsp). The data have an hourly temporal resolution. Half-hourly top-layer ST in situ observations at nine stations (mostly in Gujrat State, India) are obtained from AWS of the Indian Space Research Organization (ISRO) (https://www.mosdac.gov.in/content/aws-distribution). One-hour interval SM/ST in situ observations are also available at three micrometeorological towers (Met Tower)—Misra (85.43°E, 23.41°N), Kharagpur (87.31°E, 23.31°N), and Ranchi (85.31°E, 23.31°N). These in situ measurements are harmonized and quality controlled for outliers and implausible

Table 2
Details of In Situ Observations and Satellite-Derived and Global Analyses Used in the Study

Products	Data period used	Spatial resolution	Parameter	Temporal resolution	References
TRMM 3B42v7	1999–2015	0.25°	Rainfall	3 hr	Iguchi et al. (2000)
ESACCI	1979–2015	0.25°	Soil Moisture (SM)	1 day	Dorigo et al. (2017); Gruber et al. (2017, 2019)
SMAP	2015–2019	9 km	SM	3 hr	Entekhabi et al. (2014)
CFS	1979–2015	0.5°	SM	6 hr	Saha et al. (2014)
GLDAS	1979–2015	0.25°	SM	3 hr	Rodell et al. (2004)
FNL	1999–2015	1°	SM	6 hr	National Centers for Environmental Prediction/National Weather Service/NOAA/US Department of Commerce (2000)
LDAS	2000–2015	4 km	SM	1 hr	Osuri et al. (2017); Nayak et al. (2018)
Agromet AWS	2011–2013	48 stations (refer Figure 1a)	SM	1 hr	Bhattacharya et al. (2009)
ISRO AWS-AGRI	2011–2013	9 stations (refer Figure 1a)	Soil Temp. (ST)	.5 hr	Das et al. (2009)
BIT Misra Met tower	2011–2013	85.43°E, 23.41°N	SM and ST	1 hr	CTCZ data bank (http://www.incois.gov.in/portal/datainfo/pdctcz.jsp)
IIT Kharagpur Met Tower	2011–2013	87.31°E, 23.31°N	SM and ST	1 hr	
Ranchi Met Tower	2011–2013	85.31°E, 23.31°N	SM and ST	1 hr	

values following Dorigo et al. (2012). Along with these in situ observations, global SM analyses have also been used from various sources in this study. The SM project of the ESACCI (http://www.esa-soilmoisture-cci.org) provides a long-term combined SM product from multiple active and passive microwave sensors (Dorigo et al., 2017; Gruber et al., 2017, 2019). It is a daily product with a spatial resolution of 0.25°. The SM product from SMAP (Colliander et al., 2017) at high-resolution (9-km and 3-hr interval) is also used. Besides these products, global SM analyses have also been used in this study. The SM products obtained from (i) Climate Forecast System (CFS) developed at the NCEP (Saha et al., 2014), (ii) Global Land Data Assimilation System (GLDAS) of the National Aeronautics and Space Administration (Rodell et al., 2004), and the (iii) FNL analysis are also used. The CFS and FNL analysis are available in 6-hr interval, while GLDAS is in 3-hr interval. The regional and global analyses of SM and ST are bilinearly interpolated to the observation point for validation.

The study also uses the Version 7 TRMM multisatellite precipitation analysis (i.e., the TMPA 3B42), 3-hourly combined microwave-infrared estimates and adjusted to the rain gauge data sets (Iguchi et al., 2000). The description of the data is provided in Table 1. This product is widely used for various rainfall events and considered as one of the best products for the Indian domain (Ankur et al., 2019; Prakash et al., 2015).

4. Results

The MD cases analyzed in this study are in June and August. The onset (June) and withdrawal (September) months receive relatively less rainfall when compared with the active (July–August) months (Gadgil & Asha, 1992; Krishnamurthy & Shukla, 2000; Shrivastava et al., 2017). Figure 1b presents the mean of daily SM anomaly over central India (74–87°E, 16–26°N) from above-mentioned global and regional analysis

Table 3
Verification of SM Analyses of ESACCI, LDAS, and FNL in 6-hr Interval at 51 IMD Stations and ST at 12 Stations During Monsoon Season

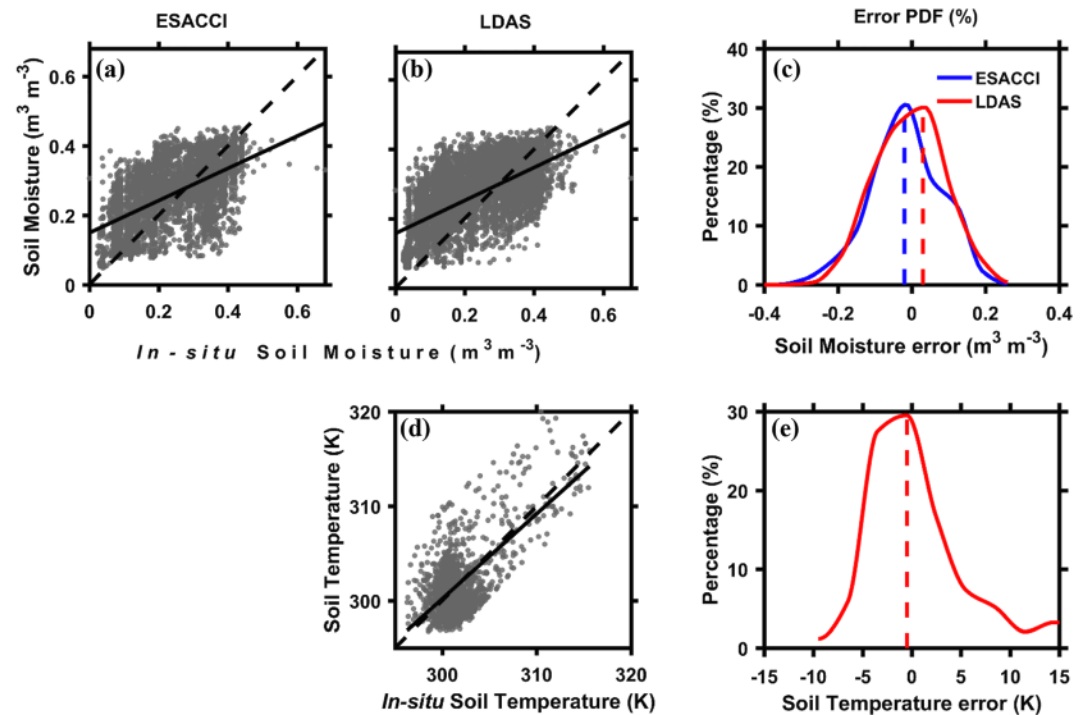|	Soil moisture (m³ m⁻³)				Soil temperature (K)	
	IMD (obs)	ESACCI-SAT	LDAS	FNL	ISRO (obs)	LDAS
Mean	0.28	0.28	0.28	0.31	303.8	302.8
SD	0.12	0.09	0.14	0.06	3.9	4.0
BIAS		0.03	0.01	0.07		−0.8
RMSE		0.09	0.09	0.11		2.7
CORR		0.54	0.65	0.53		0.74

Figure 2. Verification of top-layer SM of (a) ESACCI derived and (b) LDAS along with their (c) probability density function of SM error at 51 in situ observations (48 IMD agromet stations and 3 microtower observations). (d) Top-layer ST (K) of LDAS is verified at 12 in situ observations (nine ISRO agromet and three microtower observations) and (e) corresponding ST error PDFs for the monsoon season (June–September) of 2011–2013.

along with satellite-derived products. The climatological rainfall, as obtained from TRMM-3B42v7, is also shown in Figure 1b. Each data set exhibited signature of dry surface from May to most of the June (onset) due to relatively lesser rainfall. Later during mid-June, with increasing rains, the SM shows notably higher values. As July and August receive high monsoon rains, the surface is relatively wet with a positive anomaly in all the analyses. Note that the modest hydraulic conductivity of clay soil in central India allows higher moisture retention for longer times. Hence, the daily anomaly of SM in September remains positive as it recedes slowly. The SMAP-SM and FNL-SM anomalies show notable differences when compared with other global as well as regional products. The SM from SMAP and FNL is relatively higher in May and less during monsoon season. The SMAP-SM anomaly is prepared based on its 5 years of climatology (2015–2019).

Previous studies established the positive feedbacks between SM anomalies and atmospheric anomalies and their impact on the ST (Hardie et al., 2011; Namias, 1960; Rind, 1982; Shukla & Mintz, 1982). Considering the importance of antecedent SM on surface/near-surface temperatures, the antecedent SM conditions 15, 10, and 5 days before the formation of MD cases are analyzed to understand the land state prior to the MD formation (Kishtawal et al., 2013). The SM difference between value on the day of MD formation and the 15-, 10-, and 5-day prior-SM conditions for each MD case is used, and the average is shown for June and August cases in Figures 1c and 1d. The day of MD formation is shown in Table 1 and is considered as Day 0 or reference SM. A positive value of SM difference indicates that the surface on the day of MD formation (or the model initial time) is wet. In contrast, negative indicates drier soil as compared to prior SM conditions. It is clear that the soil is drier in June for different time lags (of 15, 10, and 5 days) and all the data sets exhibit similar behavior. The SM becomes higher from 15 to 5 days before the MD event (Figures 1c and 1d). The magnitude of SM difference varies among the data sets with values about 0.05–0.08 $m^3 m^{-3}$ for June cases (Figure 1c), and about 0–0.04 $m^3 m^{-3}$ in August (Figure 1d). It indicates that the soil is relatively wet in August than June and consistent with the rainfall and SM climatology shown in Figure 1b. It is important to note that the 15- to 10-day prior-SM conditions are nearly similar, showing a slight variation in SM difference. In comparison, the 5-day prior-SM conditions differ considerably in June (Figure 1c). In the

case of August, there is a significant change in SM conditions from 15 to 10 days, while the SM conditions are almost similar from 10 to 5 days (Figure 1d).

4.1. LDAS Verification for Indian Monsoon Season

The top-layer SM ($m^3\ m^{-3}$) is obtained from the ESACCI (SAT hereafter), and LDAS is verified against 51 in situ observatories (48 agromet stations and 3 microtower observations) at 6-hr intervals in the monsoon seasons (1 June to 30 September) of 2011–2013. The distribution of observations is shown in Figure 1a, and all the observations are within the nested domain. Figure 2 indicates the scatter diagram of SM and ST analysis and in situ observations, and corresponding error statistics are shown in Table 2. The seasonal mean and standard deviation (SD) of in situ SM observations is 0.28 and 0.12 $m^3\ m^{-3}$ (Table 2). Scatter diagram indicates that the SAT and LDAS overestimates low SM conditions and underestimates high SM conditions (Figures 2a and 2b). The satellite-derived SM analyses show a relatively high correlation (0.54) and less RMSE (~0.09 $m^3\ m^{-3}$) and bias (~0.03 $m^3\ m^{-3}$) with almost the same mean SM. The SAT analysis has limited variability (SD is ~0.09 $m^3\ m^{-3}$) and does not capture the extremes/peaks of SM over this region (Table 2). The high-resolution regional (LDAS) SM analysis is consistently better with modestly high correlation (0.65) and low RMSE and bias (~0.09 and 0.01 $m^3\ m^{-3}$). The higher SD of LDAS analyses indicates its ability to replicate SM extremes over the region during monsoon season (Table 2) as compared to satellite analyses. The mean SM error frequency distribution suggests that the ESACCI-SM error has a primary peak centered at −0.02 $m^3\ m^{-3}$ (~31%), while the LDAS SM error peaks at +0.015 $m^3\ m^{-3}$ at 35% (Figure 2c). The default SM conditions in the CNTL run are also verified with in situ measurements (Table 2). Unlike other analyses, the FNL overestimates (bias is 0.07 $m^3\ m^{-3}$) the SM, showing the seasonal mean as ~0.31 $m^3\ m^{-3}$. The SD indicates limited skill in capturing SM extremes (0.06) over this region. The seasonal mean RMSE is maximum in FNL analysis as compared to the others. Month wise, FNL analysis overestimates the SM in May–June and September (the onset and withdrawal months), while it underestimates in July–August (active monsoon months). It is consistent with the earlier result that the FNL overestimates the SM during premonsoon seasons in most parts of the region (Osuri et al., 2017).

The top-layer ST (K) is compared with in situ observations at 12 in situ stations (nine agromet stations and three microtower stations), and the distribution is shown in Figure 1a. From Figures 2d and 2e, the ST values less than 305 K typically show an agreement with in situ observations, while the higher ST values are underestimated by the LDAS (Figure 2d). The observed mean and bias of ST are ~303.8 and 3.9 K. The regional LDAS analyses showed a high correlation (0.74), and low RMSE (2.7 K) and bias (−0.8 K). Though the LDAS underestimates the ST, the SD is somewhat similar (4.0 K). From Figure 2e, the maximum error frequency distribution showed that LDAS-ST error is centered at 0 to −2 K (~30%). This further highlights the underestimation of ST from the analysis fields over the IMR.

Overall, the LDAS products (SM/ST) are closer to the observations, and satellite analyses exhibit smaller error metrics as compared to other analyses. Therefore, the satellite SM analyses can be used for the verification of model-simulated SM products in the absence of high spatiotemporal in situ measurements over this region. Similarly, the value addition due to the LDAS data is the higher spatial resolution and the ability to capture extremes in the surface conditions (higher SD). Generally, the highest (SM) values have relatively smaller spatial scales, and hence, the high resolution is desirable to provide realistic structures of SM heterogeneity. The coarser resolution tends to smooth out these fine-scale SM peaks, which change the location of surface heterogeneity boundaries and the feedback on the simulation of mesoscale fields.

4.2. Initial SM

The top-layer (0- to 10-cm depth) volumetric SM ($m^3\ m^{-3}$) from the CNTL experiment is compared against the ESACCI-SM. The differences between FASDAS and LDAS SM from the CNTL run have also been presented for the representative MD cases in Figure 3. These include Cases 1, 5, 7, and 8 corresponding to onset month (June) and active month (August) of the monsoon season. As seen in ESACCI-SM analysis, northern India is relatively drier (SM range is 0.05–0.20 $m^3\ m^{-3}$) in June cases (Figures 3a and 3i) as compared to August cases in which the SM varies between 0.3 and 0.5 $m^3\ m^{-3}$ (Figures 3e and 3m). Analyses of all cases indicate that the CNTL analysis relatively overestimates SM in the northwest and northeast parts of India (Figures 3b, 3f, 3j, and 3n) as compared to SAT-SM analysis (Figures 3a, 3e, 3i, and 3m). The difference of LDAS in Case 1 in the central to northern parts of India is negative (~0.06 $m^3\ m^{-3}$), indicative of lower
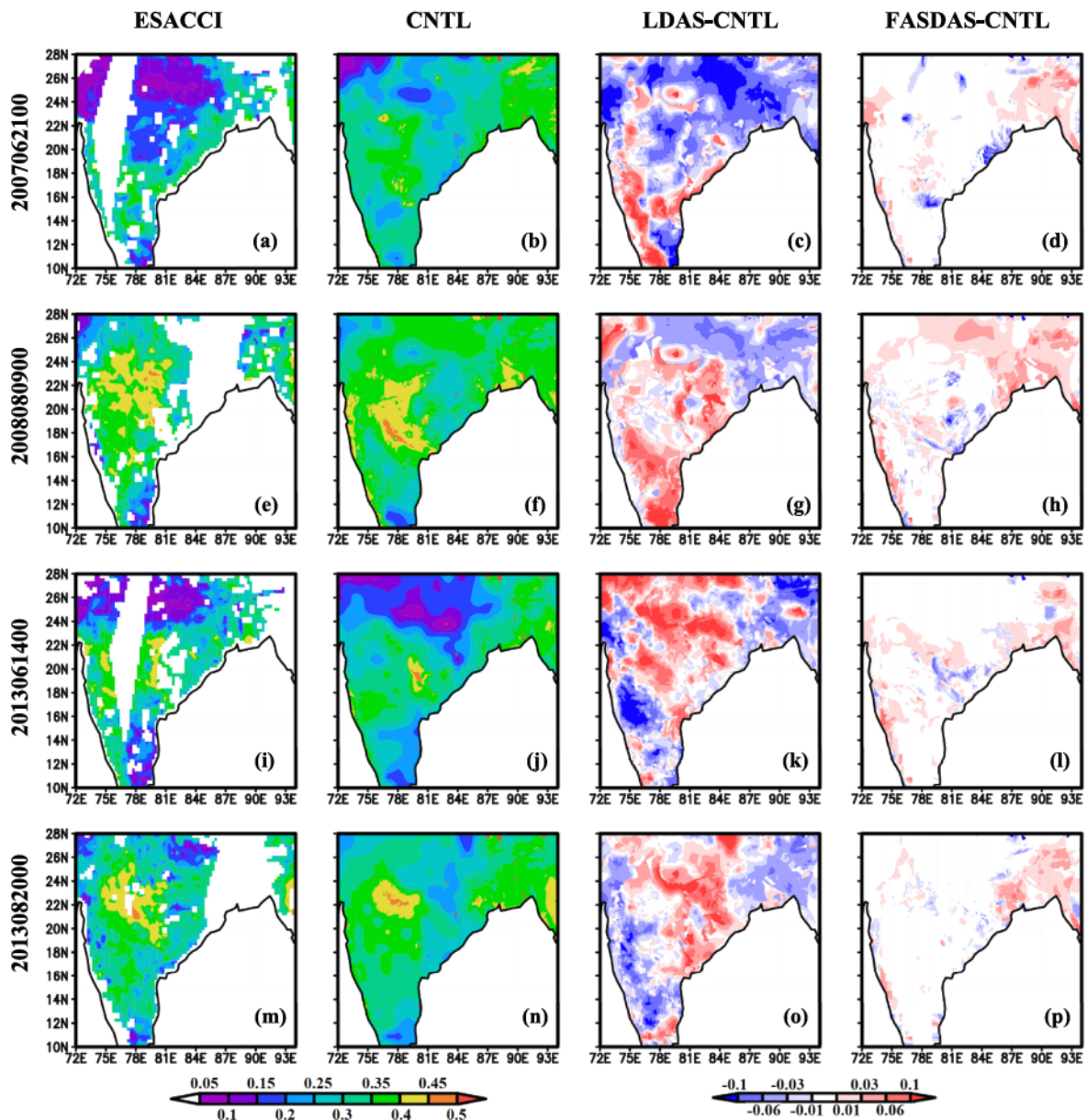
Figure 3. Spatial distribution of top-layer SM analyses from (a) ESACCI SAT, (b) CNTL, and the SM difference of (c) LDAS-CNTL and (d) FASDAS-CNTL run for Case 1. (e–h, i–l, and m–p) The same as (a)–(d) but for Cases 5, 7, and 8.

SM in the LDAS run. Overall, the LDAS appears to be close to the ESACCI-SM analysis (Figure 3c). In the case of FASDAS-SM analysis, there is minor difference across the majority of central India (± 0.01 m^3 m^{-3}). At the same time, the northeast parts show some positive difference, indicating more wet soil (Figure 3d). Considering the August case (Case 5), the LDAS shows a positive SM difference of an order of 0.05 m^3 m^{-3}, indicating wetter soil in August (Figure 3g). These results also indicate that the CNTL soil is drier, mostly in the central and southern parts of India (Figure 3f). The FASDAS analysis also exhibits positive differences mainly in the study domain, except for some parts across the east coast of India (Figure 3h). It is noteworthy that the central monsoon region is identified as an SM coupling hot spot and is dominated by clayey soil. The clay soil typically has higher moisture retention for longer times as compared to sandy soil. These features are seen in other June and August cases from the LDAS experiments. Overall, the FASDAS experiments could show little difference in SM as compared to CNTL run (Figures 3d, 3h, 3l, and 3p).
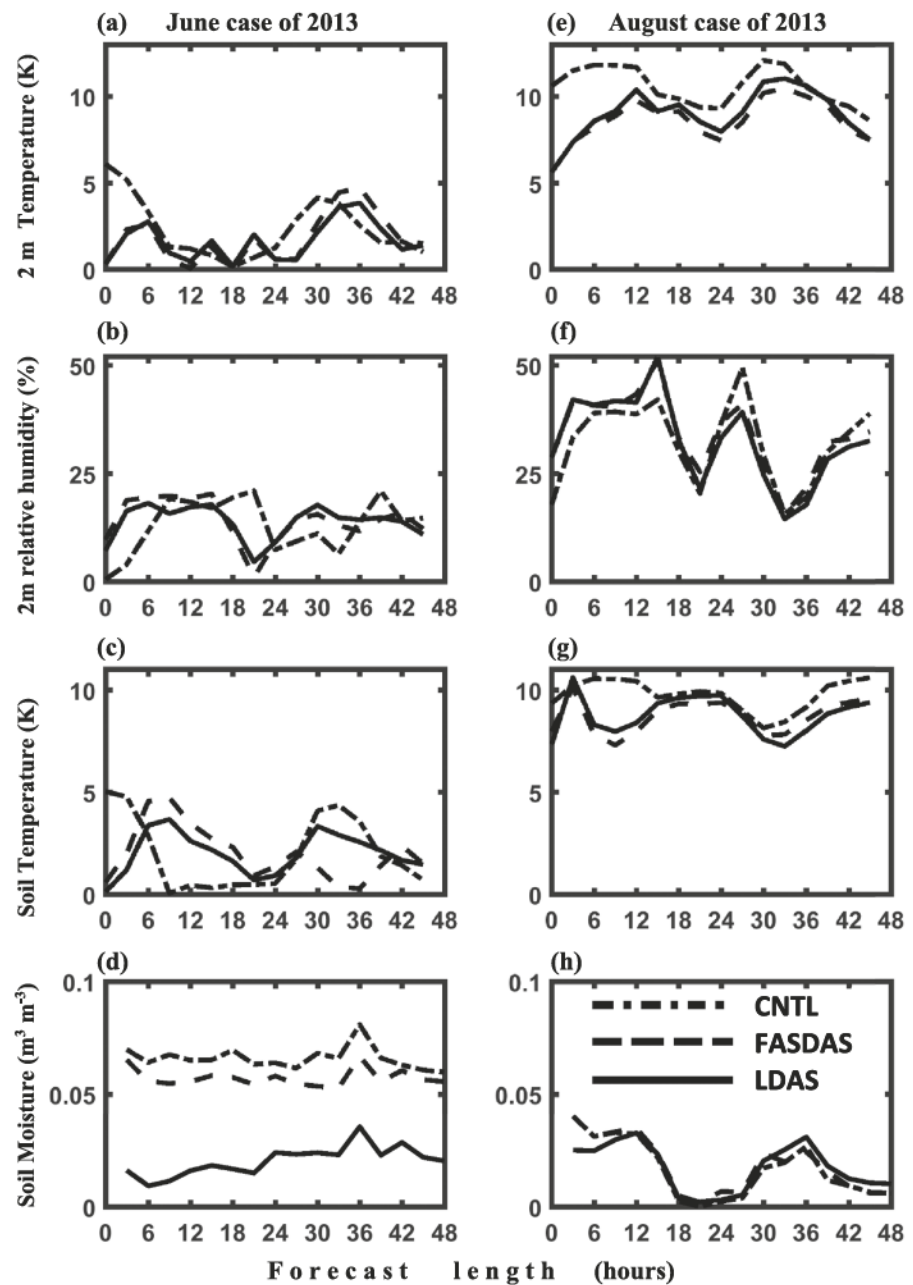
Figure 4. Mean forecast errors of (a) 2-m air temperature (K), (b) 2-m relative humidity (%), (c) soil temperature (K), and (d) soil moisture (m^3 m^{-3}) of CNTL, LDAS, and FASDAS for 2013061400 case. (e–h) The same as (a)–(d) but for the 2013082000 case.

When comparing the direct and indirect initializations, there is a considerable difference in the SM field over India, considering the CNTL-SM as reference. In the northeastern parts of India, the SM difference compared to CNTL for LDAS and FASDAS is negative and positive, respectively. It infers that the LDAS reduced the overestimation of SM, and FASDAS enhanced the SM conditions in those parts. The performance of LDAS for representing the SM in central India is consistent with the previous study (Mohanty et al., 2019; Nayak et al., 2018). Analyzing the actual SM, the LDAS appears realistic in reproducing SM heterogeneity over India during these monsoon months. The bias noticed in the CNTL-based SM is reasonably corrected in the direct initialization of SM than the indirect method. Results also show that the spatial SM loading in the LDAS is comparable with the satellite analyses, showing the minor discrepancy in spatial distribution.
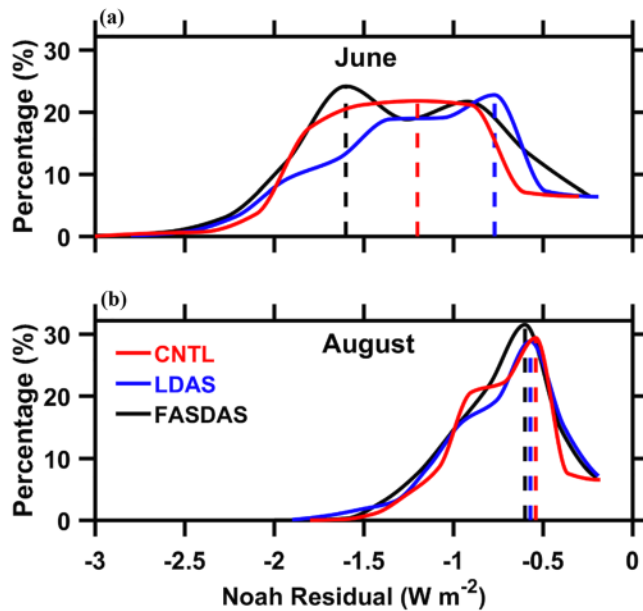
Figure 5. Probability distribution of mean residual of the surface energy budget for (a) June and (b) August MD cases considered in the study.

4.3. Evolution of Surface Fields

Surface parameters including 2-m temperature (T2), 2-m relative humidity (Rh2), ST, and SM obtained from the three experiments are compared with IMD and ISRO observations for two representative June (Case 7) and August (Case 8) cases of 2013. Note that 47 AWS stations are used in T2 and Rh2 verification 51 stations are used for SM verification and 12 stations for ST verification, based on the availability of the data. The mean errors are presented in Figure 4. There is a clear difference in error metrics by 15–30% in surface fields from June to August case for all the experiments. A common observation from these results is that the LDAS run consistently exhibited fewer errors, followed by FASDAS for most of the time. In the case of LDAS run, the mean T2 error ranges up to 3-K up to 48-hr forecast, while Rh2 and ST range within 20% and 4 K, respectively, for the June case. The FASDAS run could simulate similar errors with a slightly higher magnitude. The error of the CNTL run is more than the other two experiments most of the time. Considering the August case, the average error of surface variables (T2, Rh2, and ST) is ~15–30% that in June case, and the error difference among the runs is significant. The mean SM error (Figures 4d and 4h) revealed significant differences from June to August cases. The LDAS SM exhibited the least errors (0.01 to 0.03 $m^3\ m^{-3}$) for all forecast hours when compared with that of CNTL (>0.07 $m^3\ m^{-3}$) and FASDAS (~0.06 $m^3\ m^{-3}$) runs for June cases. In the August case, the LDAS-SM errors are comparable to that of CNTL and FASDAS runs, indicating the similar evolution of SM in all the experiments. This similarity could be because of deficit values in June (onset month) and relatively high values in August month (an active month for monsoon season) (refer Figures 1b–1d). Thus, when the land is relatively dry (less SM), the incorporation of realistic SM improves the evolution of surface parameters significantly. In contrast, when the soil is wet (for, e.g., August cases), then all the runs showed similar performance because of the high rainfall, and this leads to limited ability for improvement. Overall results illustrate how the land state impacts the evolution of surface variables.

Following Chen et al. (1996), the performance of LSM depends on the surface energy balance representation. The storage flux represented as the residual indicates the imbalance of the surface energy balance equation and is not an atmospheric or computed variable. The residual analysis builds up the confidence in the representativeness of the energy balance and has been assessed for all the experiments. Figure 5 shows the mean PDF of the area-averaged Noah residual in the MD region for June and August cases. The LDAS has lesser residual (0.75 $W\ m^{-2}$) at high frequency (~20%) in the June cases (Figure 5a). Note that the FASDAS showed two peaks of almost similar frequency at −0.9 and −1.6 $W\ m^{-2}$. CNTL showed a broader frequency distribution between −2 and −0.5 $W\ m^{-2}$ at ~20% (Figure 5a). Contrastingly, for August cases, the residual PDFs of all experiments are narrow and centered between −0.5 and −0.6 $W\ m^{-2}$ with a maximum frequency of ~30%. However, the CNTL has a secondary peak at −1 $W\ m^{-2}$, showing relatively broader PDF. Note that the PDFs are much wider in case of June cases (i.e., drier month), while they are narrow for August (wet month) cases. It could be related to the underlying as well as pre-MD antecedent SM conditions, as shown in Figures 1b–1d. Considering the spatial evolution of residual among the experiments, the improved surface conditions in the LDAS run lower the residuals in the central India and northwest part of India as compared to the other experiments. The FASDAS exhibits less residual in the northeast parts of India as compared to CNTL and LDAS (not shown). Overall analyses highlight that the LDAS simulated land-surface fields improve the net radiation energy balance. It can be inferred that the components of surface energy budget are well partitioned in the LDAS run and could be related to the realistic land surface conditions as energy partitioning over the study domain is highly sensitive to surface conditions (Douglas et al., 2006; Pielke et al., 2011).

4.4. Moisture Budget Analysis

The moisture budget terms during MD life (~48 hr) are analyzed using the atmospheric water vapor budget equation (Yoon & Huang, 2012).
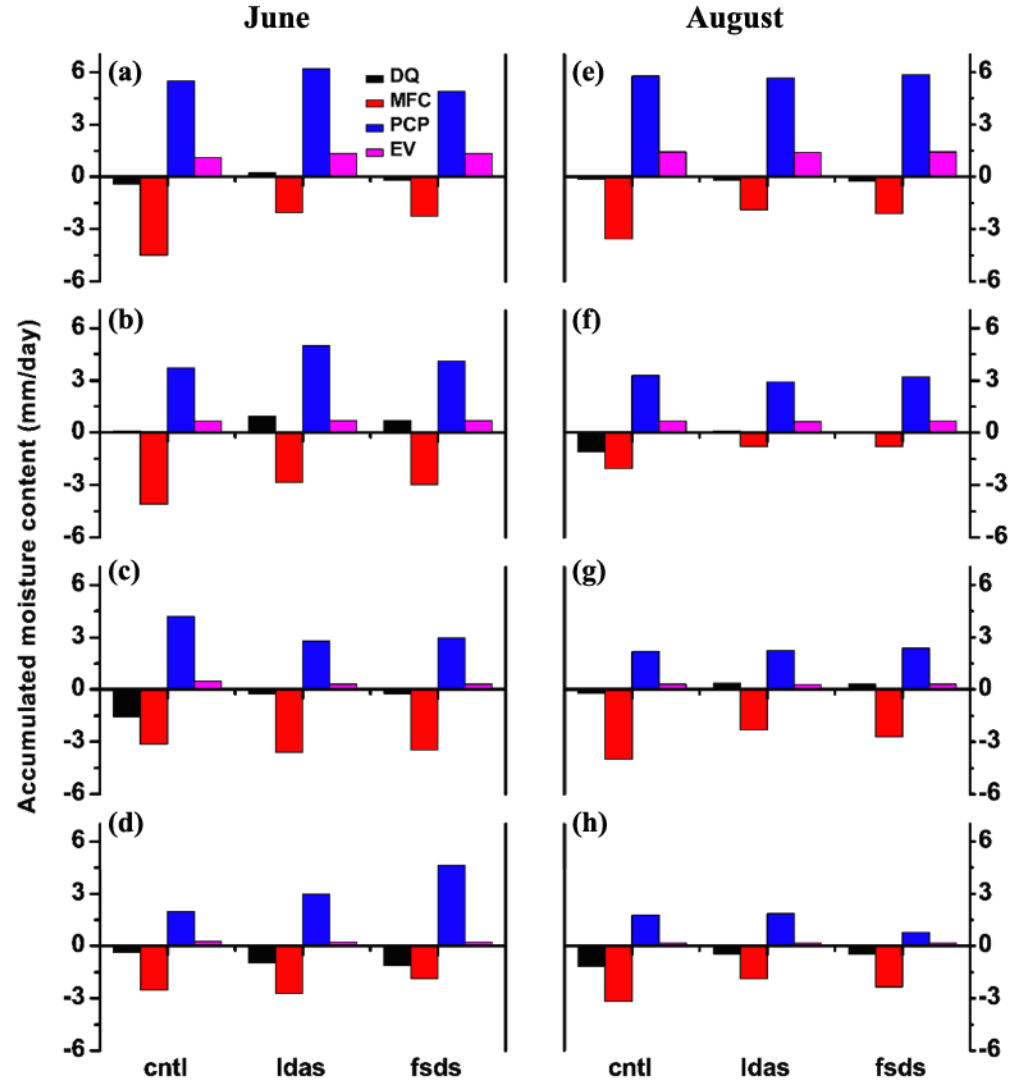
Figure 6. Model simulated average moisture budget terms (mm) such as storage term (DQ), moisture flux convergence (MFC), precipitation (PCP), and evaporation (EV) of June cases for (a) 12-hr, (b) 24-hr, (c) 36-hr, and (d) 48-hr forecasts. (e–h) The same as (a)–(d) but for August cases.

$$\frac{\partial W}{\partial t} + \nabla.\vec{Q} = EV - PCP. \tag{1}$$

Here the atmospheric precipitable water obtained from vertical integral of specific humidity (W) given as $W = \frac{1}{g}\int_{ps}^{pt} q.dp$ and $\frac{\partial W}{\partial t}$ is the storage term denoted as DQ.

Vertically integrated water vapor flux ($\vec{Q}$) is defined as $\vec{Q} = \frac{1}{g}\int_{ps}^{pt} \vec{V} q.dp$, and $\nabla.\vec{Q}$ is the horizontal convergence of vertically integrated water vapor flux, also known as moisture flux convergence (MFC). The total surface evaporation and accumulated rainfall are denoted as EV and PCP. g is the acceleration due to gravity, and ps and pt are pressure at the surface and top of the atmosphere, respectively.

Moisture budget terms are computed over a $4° \times 4°$ domain where the center of the domain represents MD center at 6-hourly time series of DQ, MFC, EV, and PCP in mm day^{-1}. Figure 6 shows the mean moisture budget terms (mm day^{-1}) from the three different experiments for the June (left column) and August (right column) cases for different forecast lengths. The variations in moisture budget terms between CNTL, LDAS, and FASDAS are different, and the PCP shows the maximum variability followed by MFC. The EV appears
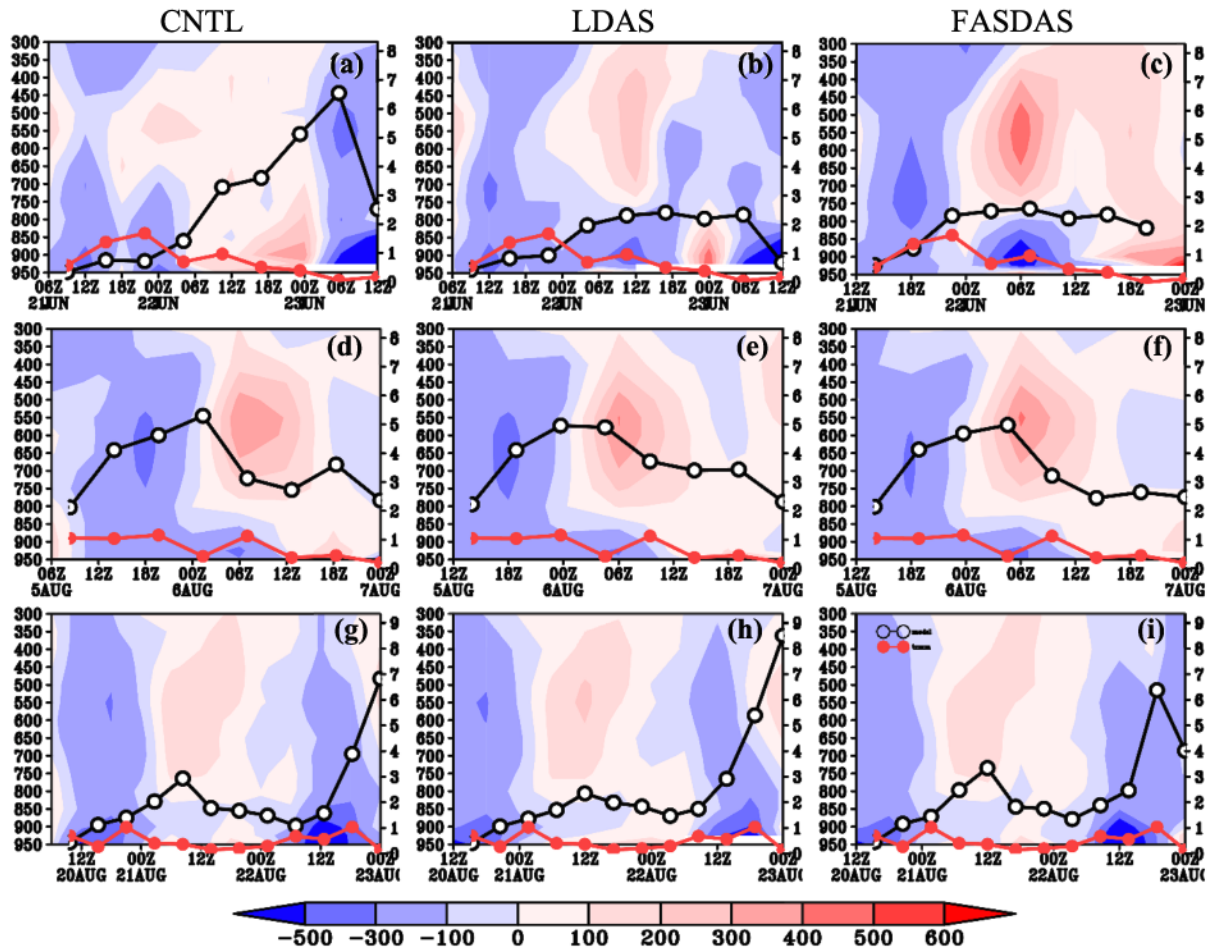
Figure 7. Time-height evolution of diabatic heating (K/s) from (a) CNTL, (b) LDAS, and (c) FASDAS runs for 2007062100 case along with model predicted rainfall (black line with open circle) and TRMM rainfall (solid red line). (d–f and g–i) The same as (a) and (b) but for 2008080500 and 2008082000 cases, respectively.

to have less contribution to the moisture fields in terms of both magnitude and variability. Overall, MFC has the largest contributing influence in the supply of moisture into the systems. It is noted that the PCP change grows in FASDAS (unlike LDAS) as forecast length increases (Figures 6a–6d) in June cases, while similar PCP changes are seen for all the August cases (Figures 6e–6h).

The domain averaged MFC magnitude is less (~2 mm) in LDAS run as compared to the CNTL (~3 mm) and FASDAS (>2 mm) for the Day 1 forecast of June cases, which then increases in subsequent simulation up to 48 hr. The patterns of PCP variability are similar to the MFC, while the EV term decreases for the same period. The local storage term (DQ) also increases with forecast length; however, the same in FASDAS exhibited a decrease with time. In the case of August, the contribution of MFC is less as compared to that in June cases. It may be due to the local effect and explained further using the land-surface feedback process.

4.5. Diabatic Heating and Rainfall Evolution

The time-height cross section of diabatic heating (K/s) averaged over a 4° × 4° box around the MD position for all the forecast hours is showed in Figure 7 along with TRMM and model rain rate. There is abundant diabatic heating in the midlevels of CNTL simulation from 18 UTC 21 June 2007 (Figure 7a), which likely contributed to the excess Day 2 onward. In case of LDAS run (Figure 7b), the higher diabatic heating is more in the middle to upper levels for 12 hr on 22 June 2007 (Day 2), which leads to the increased rain rate and subsequent decrease in the Day 3 (23 June 2007), and in agreement with the observed evolution of rainfall. The FASDAS run could improve the rainfall simulation when compared to CNTL-simulated rainfall
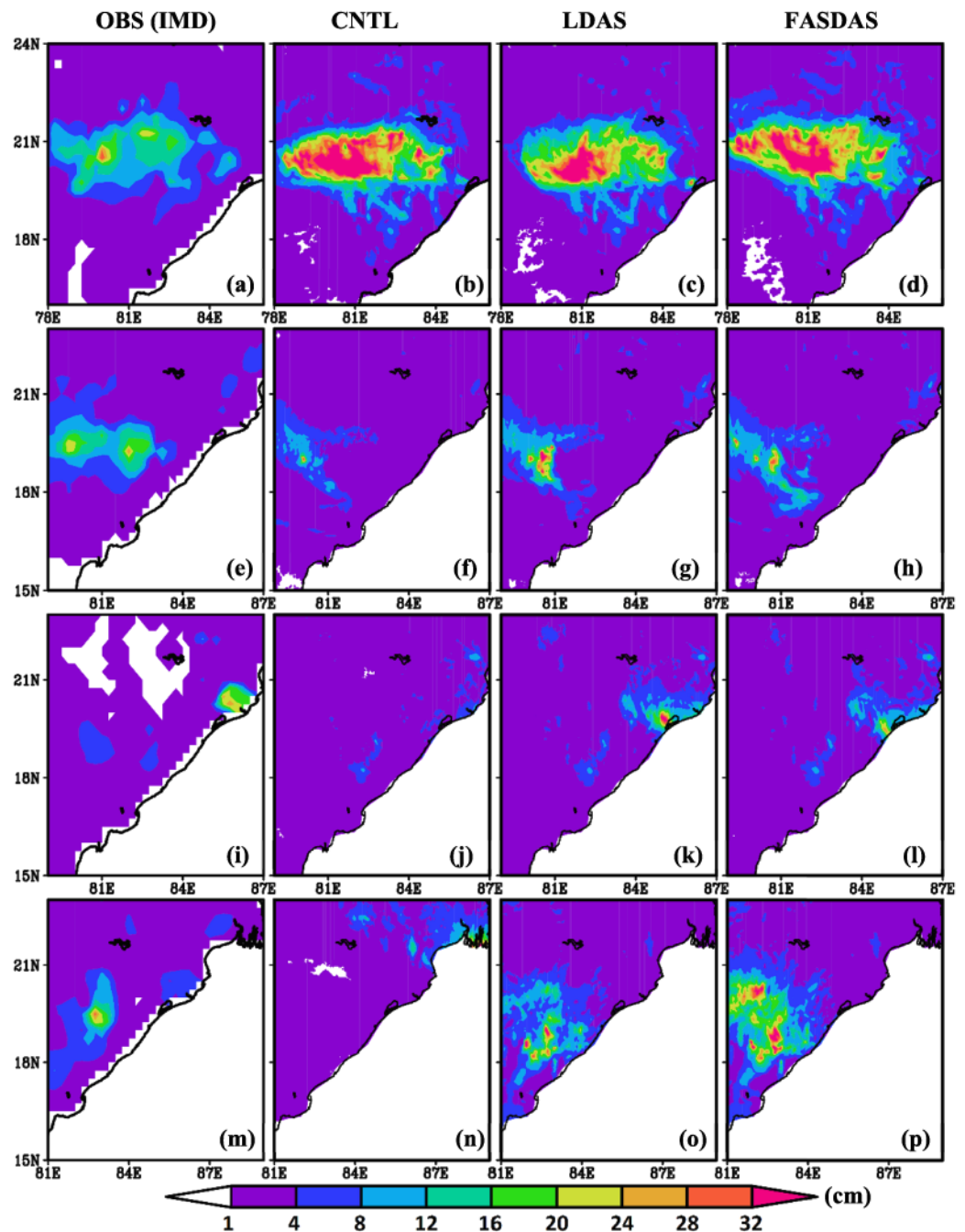
Figure 8. The 24-hr accumulated rainfall (cm) from (a) IMD, (b) CNTL, (c) LDAS, and (d) FASDAS experiments for 2007062800 case. (e–h, i–l, and m–p) The same as (a)–(d) but for 2013061400, 2007080500, and 2008080900 cases, respectively.

(Figure 7c). In the case of the August case (5–7 August 2007), the simulated rain rate evolution in all the experiments is more or less the same. The evolution of diabatic heating is also similar in these runs. The heterogeneity is represented in the land surface conditions (wet and dry/cold and warm) from the direct initialization of LDAS fields, thus to improve the rainfall simulation (Xinmin et al., 2000). As discussed, the June period is relatively dry and warm. The SM/ST initialization improved the MD simulation as well as associated rain rate. While in August month, the land surface is nearly saturated due to active monsoon conditions; therefore, the initialization of SM/ST does not show a substantial impact on MD cases.

Table 4
Mean CRA Horizontal Shifts (dx, dy, and dθ) From Three Experiments for June and August Cases.

CRA shifts	June			August		
	CNTL	FASDAS	LDAS	CNTL	FASDAS	LDAS
dx	1°	0.8°	−0.5°	1.125°	1.125°	1°
dy	−0.2°	−0.06°	0.06°	−0.37°,	0.55°	−0.3°
$dθ$	2.25°	2.5°	0.25°	5.5°	3°	5.5°

Note. "+" sign indicates right/forward/clockwise shift, and "-" sign indicates left/backward/anticlockwise shift in the rainfall threshold.

Twenty-four-hour accumulated spatial rainfall (valid for Day 1) obtained from CNTL, FASDAS, and LDAS run along with IMD rainfall for cases of June and August is presented in Figure 8. IMD analyses show two cells of maximum rainfall (20–24 and ~30 cm) that occurred on the 28–30 June 2007 case (Figure 8a). The three experiments overestimated the rainfall with similar spatial orientation; however, LDAS shows two heavy rainfall cells, unlike FASDAS. In the case of 14–17 June 2013 case (Figures 8e–8h), the rainfall distribution is more or less similar in all three cases; the rainfall amount is improved in LDAS and FASDAS runs as compared to CNTL run. In the case of 5–7 August 2007, the coastal rainfall (around 20°N) observed in the IMD rainfall analysis is 20–28 cm (Figure 8i). The CNTL run simulated scattered rainfall between ~4 and 8 cm over the same region (Figure 8j) while the LDAS run, on the other hand, computed the rainfall distribution and magnitude (~32 cm) well (Figure 8k). The FASDAS run could also show good rainfall simulation, but it is displaced southward (Figure 8l). In the case of 9–11 August 2008, the observed rainfall at 19–20°N latitudes is well reproduced in the LDAS run with slight overestimation in spatial coverage (Figure 8o). The FASDAS-simulated rainfall is distributed over a broader region with notable overestimation (Figure 8p).

4.6. Estimation of Rainfall Errors Using Contiguous Rain Area Method

Traditional statistical metrics (such as simple bias, root mean square error, RMSE) provide skill assessment of the high-resolution models for quantitative rainfall prediction. However, they do not provide direct insights into the source of errors. As an alternative, the contiguous rain area (CRA; following Ebert & McBride, 2000; Ebert & Gallus, 2009; Gilleland et al., 2010; Osuri et al., 2017) have been developed for the spatial verification (i.e., location, extent, intensity, and pattern) for the user-specified rainfall threshold (also known as CRA threshold). This method has been applied for rainfall over the IMR region (Kumar Das et al., 2014; Sharma et al., 2019). In the CRA method, the actual rainfall threshold is shifted in the x direction (left or right), y direction (forward or backward), and azimuthal direction (clockwise or anticlockwise) to achieve the best match (maximum correlation and minimum mean square difference, MSD) with the observation. This horizontal shift (in x and y direction) provides displacement errors (dx and dy, respectively), while the shift in azimuthal direction provides the rotational error ($dθ$). Similarly, the pattern error indicates the error in the distribution of rainfall, and volume error indicates the error in the amount of rain. More details on the formulation of each error can be seen in Osuri et al. (2017) and Ebert and Gallus (2009). The CRA verification of 24-hr accumulated model rainfall is carried out against IMD rainfall analyses.

Table 4 provides the mean horizontal and rotational shifts obtained from the CRA. For June cases, the LDAS exhibited a minimum mean dx shift of −0.5° as compared to CNTL (−1°) and FASDAS (0.8°). A similar pattern in mean dy shift is also noted (−0.2°, −0.06°, and 0.06°). The CNTL and FASDAS show a similar clockwise shift of 2.25° and 2.5°, while the LDAS has a minimum clockwise shift of 0.25°. In the case of the August cases, the CRA exhibited similar horizontal shifts among the experiments. The mean dx shifts in CNTL and FASDAS are the same (1.125°), while the LDAS has a 1° shift. The mean dy shifts in LDAS, CNTL, and FASDAS are, respectively, −0.3°, 0.37°, and 0.55°. The FASDAS showed a minimum rotational shift (3°) as compared to CNTL (5.5°) and FASDAS (5.5°) in the August cases.

Figure 9 provides mean displacement, pattern, volume, and rotational errors for different CRA thresholds from the three experiments for all the cases. The sum of all these error components is 100%. Following IMD classification, the categorical rainfall, such as moderate (≤ 64.4 mm day^{-1}), heavy (>64.5 to ≤ 115.5 mm day^{-1}), and very heavy (>115.6 to 204.4 mm day^{-1}) are selected as CRA thresholds. Mean statistics with 95% confidence intervals indicate that pattern error is the largest (40–50%) up to heavy rainfall (115.5 mm day^{-1}); however, the volume error contributes the maximum (40–50%) at very heavy rainfall category (204.4 mm day^{-1}) to the total error of June cases (Figures 9a–9c). The displacement error contributes more or less 20–30% to the total error. Among all, the rotational error of rainfall in the azimuthal direction is minimum (~5%) for June cases (Figures 9a–9c). In the case of August cases, the displacement and pattern errors contribute more or less similar (40–50% each) for different CRA thresholds in all the experiments (Figures 9d–9f). The volume and rotational errors are significantly less in all experiments for
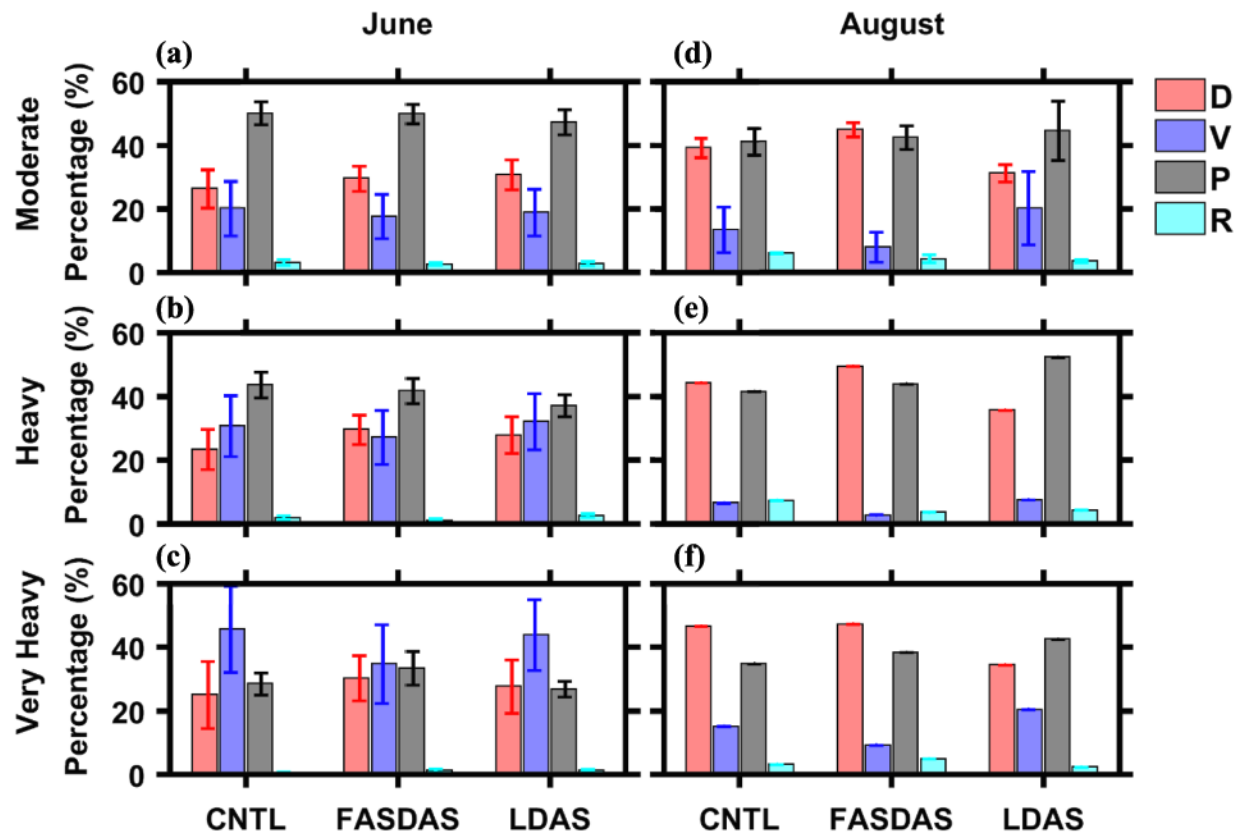
Figure 9. Rainfall error decomposition into mean displacement (*D*), volume (*V*), pattern (*P*), and rotational (*R*) errors using CRA method for different categorical rainfall (a) moderate rains ($\leq$64.4 mm day^{-1}), (b) heavy rains (>64.5 to $\leq$115.5 mm day^{-1}), and (c) very heavy rains (>115.6 to 204.4 mm day^{-1}) for June cases. (d–f) The same as (a)–(c) but for the mean of August cases.

different thresholds in August cases (Figures 9d–9f). Intercomparison of experiments, the displacement and pattern errors are relatively less in the LDAS run as compared to that of CNTL and FASDAS runs. However, the volume error is more in the LDAS compared to the others. It can be concluded that the LDAS improved the rainfall simulation in terms of location (less displacement error) and distribution (less pattern error), however, with higher error in the rainfall amount (volume error) as compared to other experiments. Moreover, the range of 95% confidence intervals is relatively less in the LDAS run for most of the error components in June cases, indicating less spread in error. However, the confidence interval is less for lower rainfall thresholds and negligible for higher rainfall thresholds. The average RMSE of moderate rainfall threshold for June cases is 26, 35, and 32 mm day^{-1} from LDAS, CNTL, and FASDAS, respectively. While for August cases, the RMSE is 62, 78, and 76 mm day^{-1} for LDAS, CNTL, and FASDAS, respectively.

Figure 10 shows different skill metrics of three experiments for the above-mentioned categorical rainfall thresholds corresponding to the June cases and August cases. The plus sign and circle symbols indicate the skill metrics before and after the CRA analysis. The accuracy of Day 1 rainfall from three experiments varies between 0.1 and 0.3 in the actual simulation (or before CRA); however, it increases to more than 0.3 after the CRA correction (Figure 10a). The Day 2 rainfall accuracy is higher than that of Day 1 in June cases. The LDAS run shows higher accuracy for Days 1 and 2 rainfall as compared to the other two experiments (Figure 10a). The bias score helps assess the overestimation or underestimation of model rainfall. The model overestimates the moderate rainfall (black symbols) while underestimates the heavy and very heavy rainfalls (blue and red color) in the actual, as well as for CRA corrected analysis in June cases. Considering the bias for August rainfall cases, the moderate and heavy rainfall is underestimated, and very heavy rain is more reliable with marginal bias (close to 1; Figure 10b). The false alarm ratio (FAR) is more than 40% in all
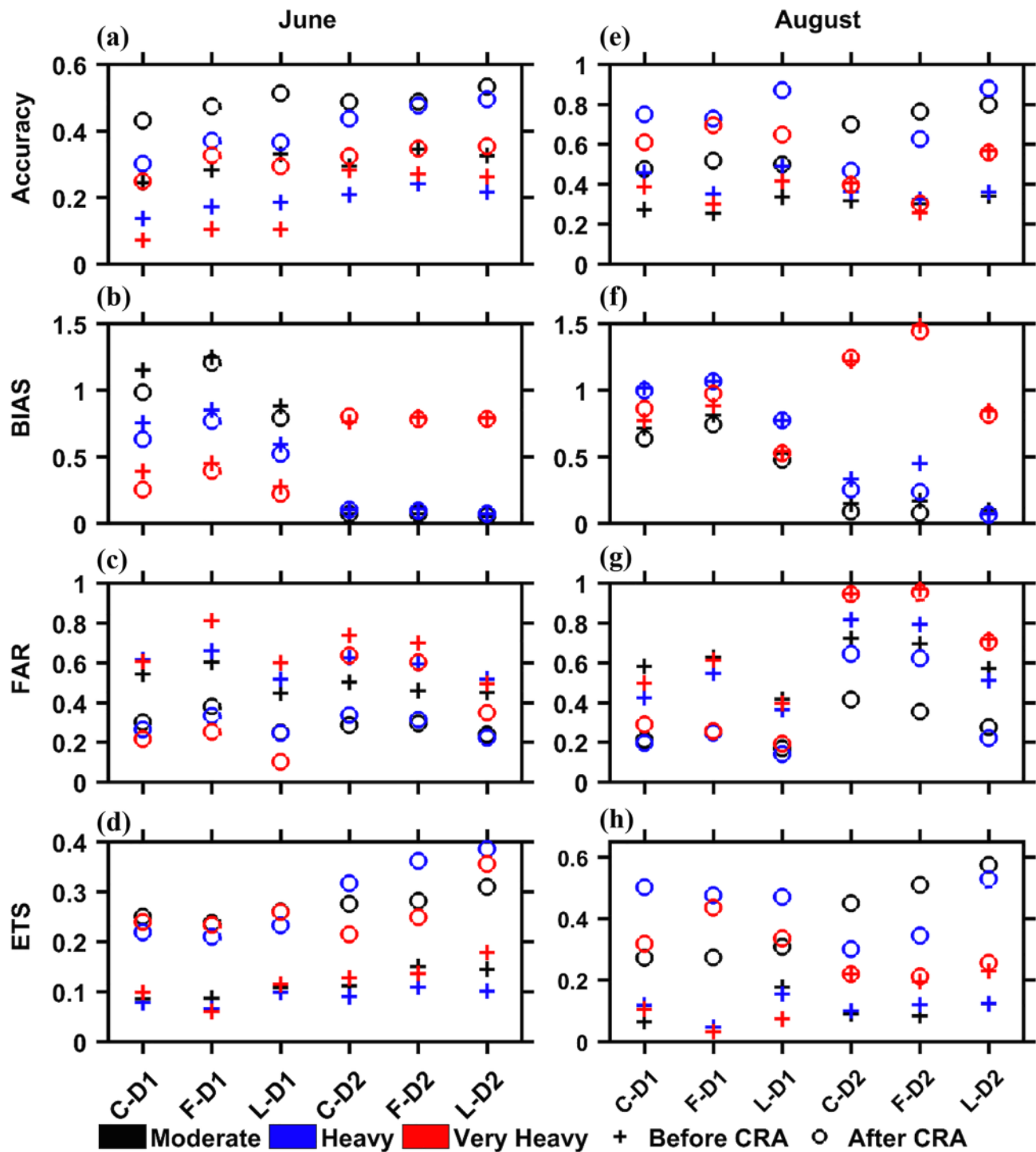
Figure 10. Mean skill scores of Days 1 and 2 model rainfall for June cases (a) accuracy, (b) BIAS (c), false alarm ratio (FAR), and (d) ETS from CNTL, FASDAS, and LDAS before the CRA (plus symbol) and after the CRA (circle symbol). (c and d) The same as (a) and (b) but for August cases. CRA thresholds considered are moderate, heavy, and very heavy rainfall categories. C-D1 and C-D2 indicate CNTL-day1 and CNTL-day2 simulations. Similarly, F-D1 and F-D2 indicate FASDAS-day1 and FASDAS-day2 simulations. L-D1 and L-D2 indicate LDAS-day1 and LDAS-day2 simulations.

the three experiments of actual rainfall; however, it reduced to 10–25% after the CRA correction in Days 1 and 2 rainfall simulation. The FAR is less in LDAS run for Days 1 and 2 rainfall as compared to the others (Figure 10c). In the actual simulation, the mean equitable threat score (ETS) lies below 0.1 for Day 1 and 0.2 for Day 2 for all the experiments. After correcting the MD rainfall to CRA displacement

errors (after CRA), the mean ETS for Day 1 rain from all the runs consistently increase to 0.2–0.3 for moderate, heavy, and very heavy rainfall categories and increases to 0.2–0.4 for Day 2 rainfall for June cases (Figure 10d). This ETS shows a definite improvement in higher rainfall thresholds (heavy to very heavy rain) for Days 1 and 2 from the LDAS run in June cases with higher ETS than the other runs (Figure 10d).

Considering the August cases (Figures 10e and 10f), the mean accuracy is higher for Day 1 actual rainfall (0.25–0.5) for different thresholds (Figure 10e) as compared to June cases (Figure 10a). After the CRA, the accuracy increases up to 0.8 in the CNTL and FASDAS, while up to 0.9 in the LDAS run for Days 1 and 2 rainfall (Figure 10e). The rainfall bias in August cases is closer to 1, indicating a marginal lower bias for all rainfall thresholds before and after CRA (Figure 10f). The actual Day 2 simulation underestimates the rainfall noticeably for moderate and heavy rain. However, the very heavy rain is overestimated in CNTL and FASDAS (BIAS > 1), while the LDAS is close to 1 (negligible bias) before and after the CRA (Figure 10f). The FAR for Day 1 actual rainfall (before CRA) is about 50%, which is reduced to 25%, and the LDAS run is better with the lowest FAR after the CRA. There is a notable difference in FAR from Day 1 rainfall to Day 2 rainfall in August cases. The FAR is more than 70% in all the experiments before CRA. After the CRA, the FAR for moderate to heavy rainfall has decreased to 40–45% in all experiments, with LDAS as the lowest one (~30%). As seen in June cases, the ETS of Day 1 rainfall of August cases before CRA is close to 0.1. After the CRA, the mean ETS has increased to more than 0.3 for the Day 1 simulation (Figure 10h).

Comparing the cases, the LDAS is again more skillful for moderate to heavy rainfall, and the FASDAS run shows a higher skill for very heavy rain. Considering the Day 2 rainfall simulation, the LDAS is consistently better for moderate rainfall after the CRA. However, the very heavy rain prediction is highly skillful for both before the CRA (ETS ~ 0.25) and after the CRA (ETS ~ 0.4) for the Day 2 simulation. Comparing June and August rainfall cases, the model bias is more for the wet August cases than the relatively dry June cases, particularly for the Day 2 rainfall simulation. The model, as compared to the June cases, does not reliably simulate the very heavy rainfall category in August cases. Moreover, the CRA horizontal shifts (in terms of dx, dy, and $d\theta$) are also higher in August cases as compared to June cases.

4.7. Surface-Precipitation Feedback

SM and atmosphere are highly coupled. There are at least two possible mechanisms for the soil-precipitation feedback (Schär et al., 1999). The rainfall over wet soils is associated predominantly with evapotranspiration (local effect). Second, the rainfall intensification is contributed by the atmospheric moisture transport (regional effect). The antecedent land state also regulates the efficiency of the precipitation processes. Here we compare the CNTL with LDAS and FASDAS, which are initialized with modified soil conditions.

The analysis of surface-precipitation feedback after the inclusion of updated land surface conditions (LDAS) and FASDAS is expected to provide additional insight into understanding the role of the land surface in modifying the precipitation. The approach here is to examine the role of the various effects that contribute to the surface-precipitation feedback mechanism (Schär et al., 1999). The precipitation changes between the experiments LDAS and CNTL (LDAS-CNTL), and FASDAS-CNTL is termed as ΔP and can be expressed as

$$\Delta P = P' - P = \underbrace{\Delta\chi(ET + IN)}_{Term\ A} + \underbrace{\chi\Delta ET}_{Term\ B} + \underbrace{\chi\Delta IN}_{Term\ C} + \underbrace{\Delta\chi(\Delta ET + \Delta IN)}_{Term\ D}, \tag{2}$$

where χ is the precipitation efficiency that is defined as the quantity of moisture that precipitates out from the moisture that enters the domain and given by $\chi = \dfrac{P}{(ET + IN)}$, where ET is evaporation, and IN is moisture influx.

Term A in Equation 2 is the efficiency effect (EE), which stands for the precipitation change due to the changes in χ in the LDAS or FASDAS runs as compared to the default CNTL run. Term B is a surface effect (SE) and represents the variation in evaporation. The Term C denotes the remote effect (RE) describing the impact of altered moisture influx on precipitation. Term D is the residual term.
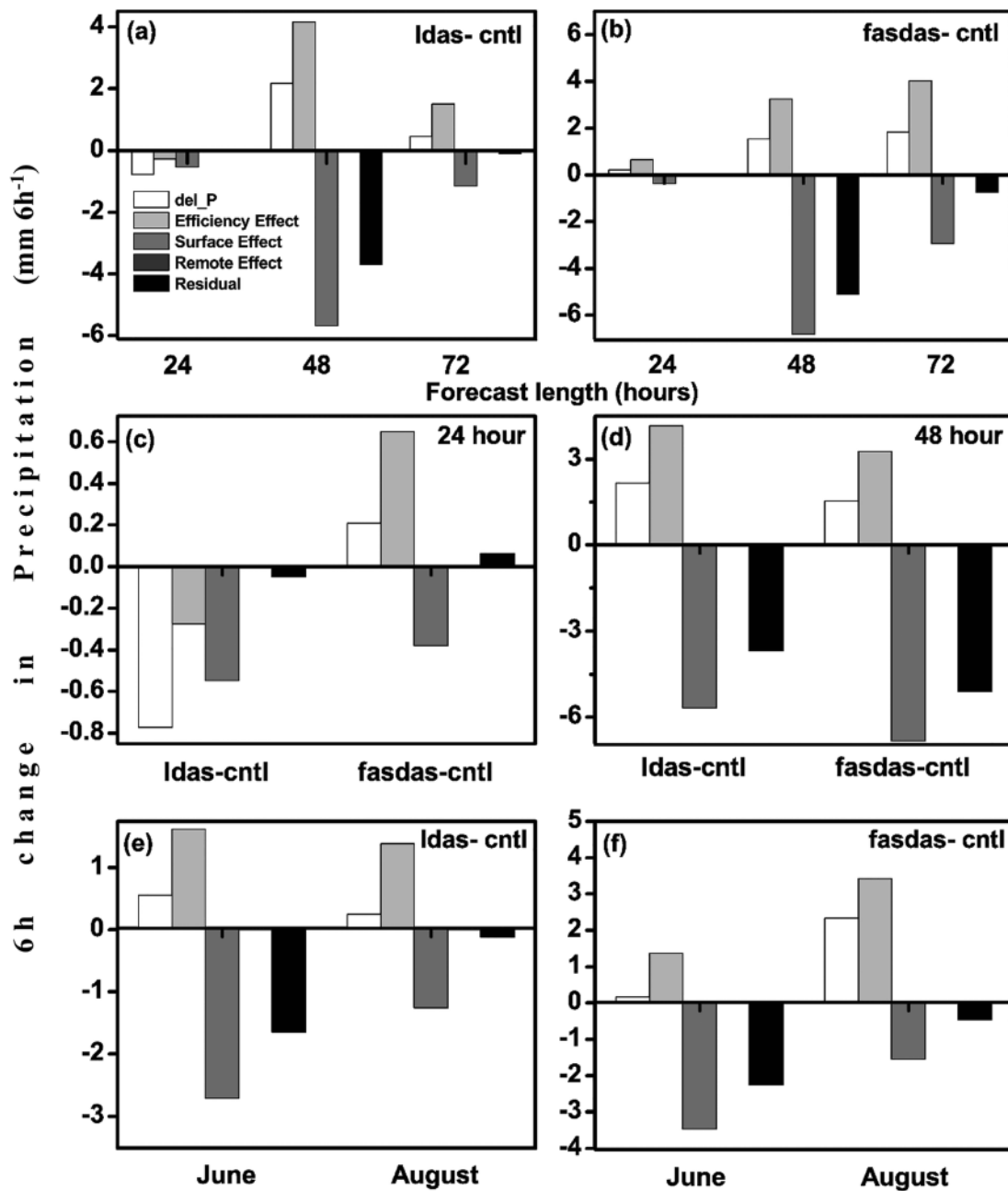
Figure 11. Changes in precipitation for (a) LDAS-CNTL and (b) FASDAS-CNTL in mm 6 hr^{-1} from all the cases. Each of the bars conveys to each term of the equation computed over the swath along the track. (c and d) The same as (a) and (b) but for the 0- to 24-hr and 24- to 48-hr average. (e and f) The same as (a) and (b) but based on June and August cases.

The surface-precipitation feedback (calculated as mm per 6 hr) is computed over an area of 200 km around the MD and is presented in Figure 11. Each term in Equation 2 is computed from the LDAS and FASDAS experiments against the base run, CNTL. Figures 11a and 11b show the mean of each term corresponding to LDAS and FASDAS, respectively, at different forecast lengths. The precipitation amount is mainly due to precipitation efficiency (χ) and SE in both the runs. The magnitude of RE is orders of magnitude smaller in terms of moisture influx (IN) in contributing precipitation.

In Figures 11c and 11d, the feedback terms have been analyzed for the forecast lengths of 24 and 48 hr. The contribution of ET toward precipitation is around 60% of the simulated changes as a whole. From Figure 11c, the LDAS-CNTL suggests that the SE is more dominant in contributing the precipitation. The negative sign
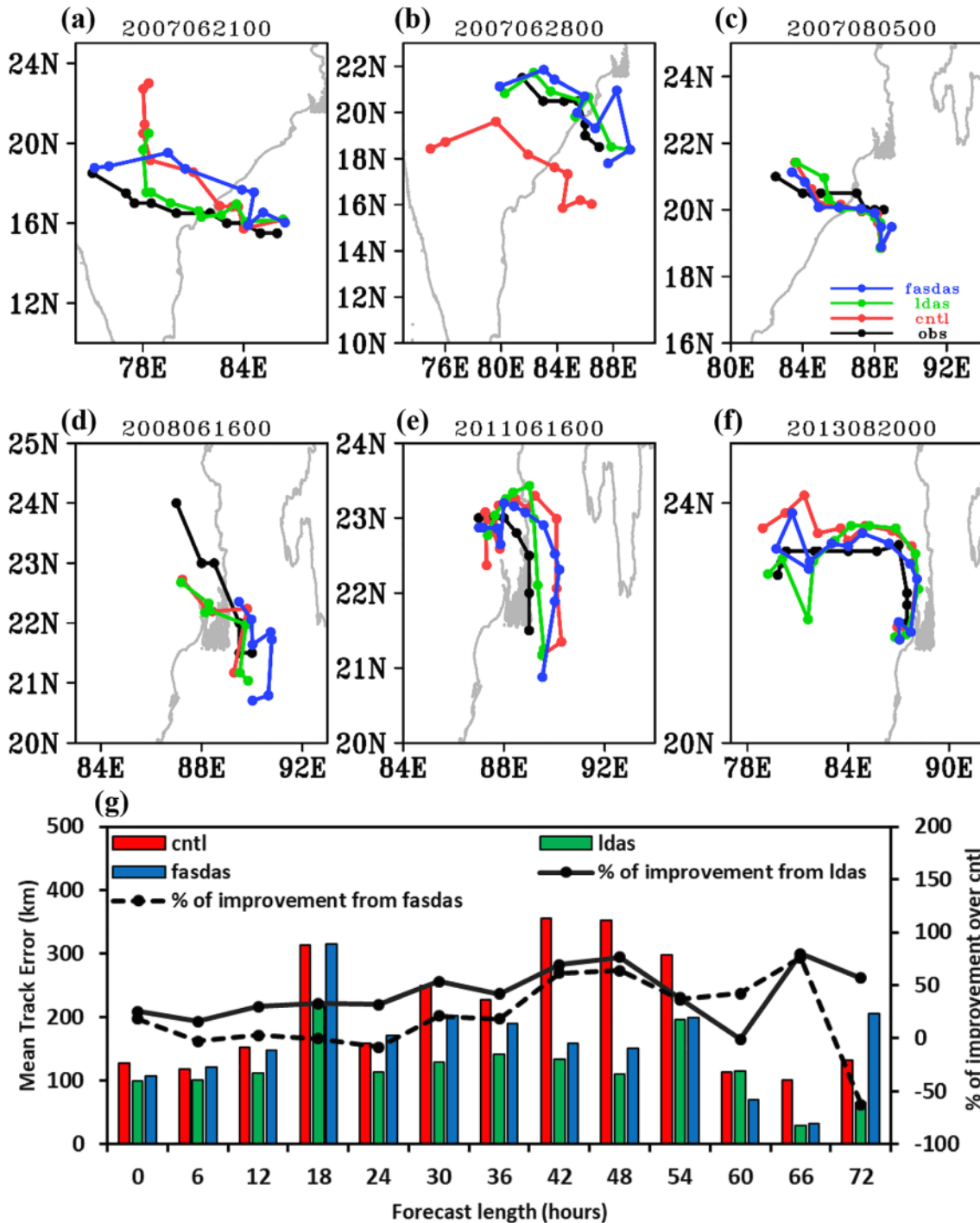
Figure 12. Model simulated tracks from CNTL, LDAS, and FASDAS along with IMD best estimates for monsoon depression cases (a) 2007062100, (b) 2007062800, (c) 2007080500, (d) 2008061600, (e) 2011061600, and (f) 2013082000. The line in the graph shows the % of improvement over CNTL from LDAS (solid line) and FASDAS (dashed line).

signifies the positive contribution of latent heat in the boundary layer toward precipitation due to evapotranspiration. In the case of FASDAS-CNTL, the EE is the more dominant term in contributing to the precipitation rate. It is due to higher SM generated by FASDAS (refer Figure 3) that reduced the Bowen's ratio with increased latent heat flux into the boundary layer. The net effect is a shallower boundary layer, thus increasing moist static energy per unit mass and an enhanced rate of moist convection in the atmosphere. Similar results can be noted in Figures 11e and 10f (monthwise analysis).

Interestingly, the effect/sensitivity of each term is more for the relatively dry June as compared to relatively wet August cases in case of LDAS run (Figure 11e), unlike FASDAS (Figure 11f). The contribution of evaporation change (SE term) is more in June as compared to that in August and could be the fact that the SM is evaporated more in June due to its drier and hotter land surface conditions. This is opposite for August cases, and hence, the SE term is weaker (Figure 11e). It could be the reason for the relatively higher impact of land surface conditions for June cases, as stated in the previous sections.

4.8. Track and Intensity

Model-simulated tracks of the MD cases are shown in Figure 12 from the CNTL, FASDAS, and LDAS experiments along with the best-estimated track. The overall track prediction by LDAS is reasonably good when compared with CNTL. The initial position for both the experiments shows similarity and is 57 km away from the observed location. The inland movement of the MDs is different among the experiments with underlying land surface conditions. The realistic representation of heterogeneity in land surface values (SM and ST) in the LDAS experiment in June likely caused notable improvement in track simulation, followed by FASDAS. The CNTL run shows the MD track has significantly deviated from observation, resulted in higher position errors. Considering August cases, consistent with the discussion presented earlier, all the runs show relatively similar performance. The track errors from the CNTL run are approximately 153, 159, 227, 352, 114, and 132 km for the 12- to 72-hr forecast in 12-hr intervals, while the same errors in the LDAS run are about 111, 113, 141, 110, 115, and 64 km. For the same forecast intervals, the FASDAS exhibited track errors of 149, 171, 190, 151, 71, and 206 km (Figure 12g). The gain in skill over from LDAS over CNTL is 32%, 76%, and 57% for 24, 48, and 72 hr, respectively. The FASDAS is better up to 48-hr forecast with improvement, but the longer forecast showed some deterioration with a high negative skill (Figure 12g). The CNTL-simulated MDs tracks toward higher latitudes due to the overestimation of SM content in the northern parts of India (including northeast and northwest parts; Figure 3). The track bias has been reduced in the LDAS run with the movement closer to the observed track.

5. Conclusions

The impact of SM/ST initialization and land surface conditions on inland moving depressions over the IMR is studied. The land surface conditions are updated by initializing the ARW model with off-line SM/ST fields using LDAS (direct method) and by flux-adjusting surface data assimilation (indirect methods). A 3-year-long verification of SM (at 51 stations) and ST (at 12 stations) demonstrated that the SM/ST products obtained from LDAS over the IMR have a reasonable agreement and are a value addition to the satellite-derived SM for spatial characteristics. Eight MD cases are studied, and the following broad conclusions are drawn.

The land surface is relatively drier 15 to 10 days prior to MD formation in June than that of the August MD cases. That is, the SM is relatively high in August due to active rains. These SM anomalies show positive feedbacks and impact the ST in the domain. The direct and indirect initializations exhibited a considerable difference in the initial SM field over India as compared to the CNTL analysis. The representation of initial SM in the model through indirect initialization (FASDAS) is almost similar or comparable with that of CNTL analysis. The bias in the CNTL SM is corrected in the direct initialization of SM relative to the indirect method, reducing the overestimation in the northeastern parts of India and central India. Moreover, the LDAS is more realistic in replicating the initial SM heterogeneity over India and is close to the observation.

In the case of the LDAS experiment, the diabatic heating is well represented in agreement with the observed rainfall, unlike the CNTL run. The FASDAS run also showed a realistic evolution of rains. The local term and moisture convergence terms contribute more to the moisture budget, and the direct initialization of SM/ST exhibited more impact on these terms than the FASDAS and CNTL.

Overall, mean CRA errors indicate that the pattern errors contribute more to the total rainfall error. However, the contribution from displacement and volume errors vary with rainfall threshold in June and August cases. The rotational error is the least contributor to the total rainfall error in these months. Comparing model performance in June and August months, the model is more skillful in simulating rainfall associated with June MD cases (high ETS) as compared to that of August cases (less ETS), particularly for the Day 2 rainfall simulation. After correcting the actual rainfall using CRA shifts, the ETS of Day 2 rainfall in

June cases has increased significantly from 0.17 to 0.37. In the case of August cases, the ETS is almost similar, showing no noticeable change in rainfall simulation after the CRA correction. Comparison of individual experiments, the LDAS is again consistently better than others for all rainfall categories. The direct initialization of SM/ST fields through LDAS could improve the location (less displacement error) and distribution (less pattern error) of rainfall; however, the rainfall amount (volume error) is higher as compared to other experiments. The CRA shift in the LDAS run is found to be less when compared to CNTL and FASDAS. It indicates the improved skill in reproducing the physical processes through direct initialization of high-resolution land conditions to improving rainfall distribution and location over the Indian monsoon domain.

Analyzing the surface-precipitation feedback for the MD cases, it is observed that LDAS exerts more SE than FASDAS for land coupling and is likely due to the direct initialization of surface fields. The enhanced evaporation in the LDAS due to the realistic representation of SM and ST resulted in better precipitation efficiency. Although FASDAS aided higher evaporation rates, the weaker SE led to unrealistic precipitation changes over the land.

Direct and indirect initialization of the surface fields improved the overall simulation of MDs in terms of both track and rainfall when compared with CNTL. The high-resolution, realistic LDAS land surface initial conditions aid the evolution of accurate surface variables with fewer errors. The mean track forecast errors are about ~350 km for the 3-day forecast of CNTL run. The LDAS-based SM/ST initialization improved track forecast limiting errors to 113 km for the same forecast lengths yielding an improvement of ~60% over CNTL run. On the other hand, the FASDAS run shows track errors up to ~200 km (improvement of 40–50%).

There are still some discrepancies in the simulation of surface fields and associated rainfall amount and distribution. The discrepancies can be potentially decreased by incorporating regional forcing fields to drive the LDAS and "tuning" the surface-atmospheric coupling strength (Zheng et al., 2015). The FASDAS correction terms could be recalibrated for the advection effects for large-scale events such as MDs and tropical cyclones and will be a part of a future study.

Data Availability Statement

The data associated with this work will be accessible through online, collaborative data-sharing platform of Purdue University Research Repository (https://purr.purdue.edu/publications/3536/1, doi: 10.4231/5XRA-JZ80) to support data citation, quality, and reuse by the scientific community.

References

Alapaty, K., Niyogi, D., Chen, F., Pyle, P., Chandrasekar, A., & Seaman, N. (2008). Development of the flux-adjusting surface data assimilation system for mesoscale models. *Journal of Applied Meteorology and Climatology*, *47*(9), 2331–2350. https://doi.org/10.1175/2008JAMC1831.1

Alapaty, K., Seaman, N. L., Niyogi, D. S., & Hanna, A. F. (2001). Assimilating surface data to improve the accuracy of atmospheric boundary layer simulations. *Journal of Applied Meteorology*, *40*(11), 2068–2082. https://doi.org/10.1175/1520-0450(2001)040<2068:ASDTIT>2.0.CO;2

Andersen, T. K., Radcliffe, D. E., & Shepherd, J. M. (2013). Quantifying surface energy fluxes in the vicinity of inland-tracking tropical cyclones. *Journal of Applied Meteorology and Climatology*, *52*(12), 2797–2808. https://doi.org/10.1175/JAMC-D-13-035.1

Andersen, T. K., & Shepherd, J. M. (2014). A global spatiotemporal analysis of inland tropical cyclone maintenance or intensification. *International Journal of Climatology.*, *34*(2), 391–402. https://doi.org/10.1002/joc.3693

Ankur, K., Busireddy, N. K. R., Osuri, K. K., & Niyogi, D. (2019). On the relationship between intensity changes and rainfall distribution in tropical cyclones over the North Indian Ocean. *International Journal of Climatology*, *40*(4), 2015–2025. https://doi.org/10.1002/joc.6315

Baisya, H., Pattnaik, S., & Rajesh, P. V. (2017). Land surface-precipitation feedback analysis for a landfalling monsoon depression in the Indian region. *Journal of Advances in Modeling Earth Systems*, *9*, 712–726. https://doi.org/10.1002/2016MS000829

Bhattacharya, B.K., Dutt, C.B.S. & Parihar, J.S. (2009). INSAT uplinked Agromet Station—A scientific tool with a network of automated micrometeorological measurements for soil canopy-atmosphere feedback studies. In ISPRS archives XXXVIII-8/W3 workshop proceedings: Impact of climate change on agriculture (pp. 72-77).

Bhowmik, S. R., Joardar, D., & Hatwar, H. R. (2007). Evaluation of precipitation prediction skill of IMD operational NWP system over Indian monsoon region. *Meteorology and Atmospheric Physics*, *95*(3–4), 205–221. https://doi.org/10.1007/s00703-006-0198-3

Bosilovich, M. G., Rixen, M., van Oevelen, P., Asrar, G., Compo, G., Onogi, K., et al. (2012). Report of the 4th World Climate Research Programme International Conference on Reanalyses

Bozeman, M. L., Niyogi, D., Gopalakrishnan, S., Marks, F. D., Zhang, X., & Tallapragada, V. (2012). An HWRF-based ensemble assessment of the land surface feedback on the post-landfall intensification of Tropical Storm Fay (2008). *Natural Hazards*, *63*(3), 1543–1571. https://doi.org/10.1007/s11069-011-9841-5

Chang, H. I., Kumar, A., Niyogi, D., Mohanty, U. C., Chen, F., & Dudhia, J. (2009). The role of land surface processes on the mesoscale simulation of the July 26, 2005 heavy rain event over Mumbai, India. *Global and Planetary Change*, *67*(1–2), 87–103. https://doi.org/10.1016/j.gloplacha.2008.12.005

Chang, H. I., Niyogi, D., Kumar, A., Kishtawal, C. M., Dudhia, J., Chen, F., et al. (2009). Possible relation between land surface feedback and the post-landfall structure of monsoon depressions. *Geophysical Research Letters*, *36*, L15826. https://doi.org/10.1029/2009GL037781

Charusombat, U., Niyogi, D., Garrigues, S., Olioso, A., Marloie, O., Barlage, M., et al. (2012). Noah-GEM and Land Data Assimilation System (LDAS) based downscaling of global reanalysis surface fields: Evaluations using observations from a CarboEurope agricultural site. *Computers and Electronics in Agriculture*, *86*, 55–74. https://doi.org/10.1016/j.compag.2011.12.001

Chen, F., Manning, K. W., LeMone, M. A., Trier, S. B., Alfieri, J. G., Roberts, R., et al. (2007). Description and evaluation of the characteristics of the NCAR high-resolution land data assimilation system. *Journal of Applied Meteorology and Climatology*, *46*(6), 694–713. https://doi.org/10.1175/JAM2463.1

Chen, F., Mitchell, K., Schaake, J., Xue, Y., Pan, H. L., Koren, V., et al. (1996). Modeling of land surface evaporation by four schemes and comparison with FIFE observations. *Journal of Geophysical Research*, *101*(D3), 7251–7268. https://doi.org/10.1029/95JD02165

Colliander, A., Jackson, T. J., Bindlish, R., Chan, S., Das, N., Kim, S. B., et al. (2017). Validation of SMAP surface soil moisture products with core validation sites. *Remote Sensing of Environment*, *191*, 215–231. https://doi.org/10.1016/j.rse.2017.01.021

Das, A., Ghosh, P.K., Choudhury, B.U., Patel, D.P., Munda, G.C., Ngachan, S.V. & Chowdhury, P. (2009). Climate change in North East India: Recent facts and events—Worry for agricultural management. In *Proceedings of the workshop on impact of climate change on agriculture* (pp. 32-37).

Dastoor, A., & Krishnamurti, T. N. (1991). The landfall and structure of a tropical cyclone: The sensitivity of model predictions to soil moisture parameterizations. *Boundary-Layer Meteorology*, *55*(4), 345–380. https://doi.org/10.1007/bf00119809

Dorigo, W., de Jeu, R., Chung, D., Parinussa, R., Liu, Y., Wagner, W., & Fernández-Prieto, D. (2012). Evaluating global trends (1988–2010) in harmonized multi-satellite surface soil moisture. *Geophysical Research Letters*, *39*, L18405. https://doi.org/10.1029/2012GL052988

Dorigo, W., Wagner, W., Albergel, C., Albrecht, F., Balsamo, G., Brocca, L., et al. (2017). ESACCI soil moisture for improved Earth system understanding: State-of-the art and future directions. *Remote Sensing of Environment*, *203*, 185–215. https://doi.org/10.1016/j.rse.2017.07.001

Douglas, E. M., Niyogi, D., Frolking, S., Yeluripati, J. B., Pielke, R. A. Sr., Niyogi, N., et al. (2006). Changes in moisture and energy fluxes due to agricultural land use and irrigation in the Indian Monsoon Belt. *Geophysical Research Letters*, *33*, L14403. https://doi.org/10.1029/2006GL026550

Drusch, M. (2007). Initializing numerical weather prediction models with satellite-derived surface soil moisture: Data assimilation experiments with ECMWF's Integrated Forecast System and the TMI soil moisture data set. *Journal of Geophysical Research*, *112*, D03102. https://doi.org/10.1029/2006JD007478

Ebert, E. E., & Gallus, W. A. Jr. (2009). Toward better understanding of the contiguous rain area (CRA) method for spatial forecast verification. *Weather and Forecasting*, *24*(5), 1401–1415. https://doi.org/10.1175/2009WAF2222252.1

Ebert, E. E., & McBride, J. L. (2000). Verification of precipitation in weather systems: Determination of systematic errors. *Journal of Hydrology*, *239*(1–4), 179–202. https://doi.org/10.1016/S0022-1694(00)00343-7

Ek, M. B., Mitchell, K. E., Lin, Y., Rogers, E., Grunmann, P., Koren, V., et al. (2003). Implementation of Noah land surface model advances in the National Centers for Environmental Prediction operational mesoscale Eta model. *Journal of Geophysical Research*, *108*(D22), 2002JD003296. https://doi.org/10.1029/2002JD003296

Entekhabi, D., Yueh, S., O'Neill, P.E., Kellogg, K.H., Allen, A., Bindlish, R., et al. (2014). *SMAP handbook—Soil moisture active passive: Mapping soil moisture and freeze/thaw from space*. JPL Publication; Pasadena, CA. Web Available at https://media.asf.alaska.edu/uploads/smap%20pdf/smap_handbook.pdf

Gadgil, S., & Asha, G. (1992). Intraseasonal variation of the summer monsoon. *Journal of the Meteorological Society of Japan. Ser. II*, *70*(1B), 517–527.

Gilleland, E., Ahijevych, D. A., Brown, B. G., & Ebert, E. E. (2010). Verifying forecasts spatially. *Bulletin of the American Meteorological Society*, *91*(10), 1365–1376. https://doi.org/10.1175/2010BAMS2819.1

Gruber, A., Dorigo, W. A., Crow, W., & Wagner, W. (2017). Triple collocation-based merging of satellite soil moisture retrievals. *IEEE Transactions on Geoscience and Remote Sensing*, *55*(12), 6780–6792. https://doi.org/10.1109/TGRS.2017.2734070

Gruber, A., Scanlon, T., Schalie, R. V. D., Wagner, W., & Dorigo, W. (2019). Evolution of the ESA CCI soil moisture climate data records and their underlying merging methodology. *Earth System Science Data*, *11*(2), 717–739. https://doi.org/10.5194/essd-11-717-2019

Hardie, M. A., Cotching, W. E., Doyle, R. B., Holz, G., Lisson, S., & Mattern, K. (2011). Effect of antecedent soil moisture on preferential flow in a texture-contrast soil. *Journal of Hydrology*, *398*(3–4), 191–201. https://doi.org/10.1016/j.jhydrol.2010.12.008

Holt, T. R., Niyogi, D., Chen, F., Manning, K., LeMone, M. A., & Qureshi, A. (2006). Effect of land–atmosphere interactions on the IHOP 24–25 May 2002 convection case. *Monthly Weather Review*, *134*(1), 113–133. https://doi.org/10.1175/MWR3057.1

Hunt, K. M., & Fletcher, J. K. (2019). The relationship between Indian monsoon rainfall and low-pressure systems. *Climate Dynamics*, *53*(3-4), 1859–1871. 1–13

Hunt, K. M., & Turner, A. G. (2017). The effect of soil moisture perturbations on Indian monsoon depressions in a numerical weather prediction model. *Journal of Climate*, *30*(21), 8811–8823. https://doi.org/10.1175/JCLI-D-16-0733.1

Iguchi, T., Kozu, T., Meneghini, R., Awaka, J., & Okamoto, K. I. (2000). Rain-profiling algorithm for the TRMM precipitation radar. *Journal of Applied Meteorology*, *39*(12), 2038–2052.

Jamshidi, S., Zand-Parsa, S., Kamgar-Haghighi, A. A., Shahsavar, A. R., & Niyogi, D. (2020). Evapotranspiration, crop coefficients, and physiological responses of citrus trees in semi-arid climatic conditions. *Agricultural Water Management*, *227*, 105,838.

Jamshidi, S., Zand-Parsa, S., Naghdyzadegan Jahromi, M., & Niyogi, D. (2019). Application of a simple Landsat-MODIS fusion model to estimate evapotranspiration over a heterogeneous sparse vegetation region. *Remote Sensing*, *11*(7), 741. https://doi.org/10.3390/rs11070741

Jamshidi, S., Zand-parsa, S., Pakparvar, M., & Niyogi, D. (2019). Evaluation of evapotranspiration over a semiarid region using multiresolution data sources. *Journal of Hydrometeorology*, *20*(5), 947–964. https://doi.org/10.1175/JHM-D-18-0082.1

Kellner, O., Niyogi, D., Lei, M., & Kumar, A. (2012). The role of anomalous soil moisture on the inland reintensification of Tropical Storm Erin (2007). *Natural Hazards*, *63*(3), 1573–1600. https://doi.org/10.1007/s11069-011-9966-6

Kishtawal, C. M., Niyogi, D., Rajagopalan, B., Rajeevan, M., Jaiswal, N., & Mohanty, U. C. (2013). Enhancement of inland penetration of monsoon depressions in the Bay of Bengal due to prestorm ground wetness. *Water Resources Research*, *49*, 3589–3600. https://doi.org/10.1002/wrcr.20301

Kishtawal, C. M., Niyogi, D., Tewari, M., Pielke, R. A. Sr., & Shepherd, J. M. (2010). Urbanization signature in the observed heavy rainfall climatology over India. *International Journal of Climatology*, *30*(13), 1908–1916. https://doi.org/10.1002/joc.2044

Koster, R. D., Dirmeyer, P. A., Guo, Z., Bonan, G., Chan, E., Cox, P., et al. (2004). Regions of strong coupling between soil moisture and precipitation. *Science*, *305*(5687), 1138–1140. https://doi.org/10.1126/science.1100217

Krishnamurthy, V., & Shukla, J. (2000). Intraseasonal and interannual variability of rainfall over India. *Journal of Climate*, *13*(24), 4366–4377. https://doi.org/10.1175/1520-0442(2000)013<0001:IAIVOR>2.0.CO;2

Kumar Das, A., Bhowmick, M., Kundu, P. K., & Roy Bhowmik, S. K. (2014). Verification of WRF rainfall forecasts over India during monsoon 2010: CRA method. *Geofizika*, *31*(2), 105–126. https://doi.org/10.15233/gfz.2014.31.6

Lei, M., Niyogi, D., Kishtawal, C., Pielke, R. A. Sr., Beltrán-Przekurat, A., Nobis, T. E., & Vaidya, S. S. (2008). Effect of explicit urban land surface representation on the simulation of the 26 July 2005 heavy rain event over Mumbai, India. *Atmospheric Chemistry and Physics*, *8*(20), 5975–5995. https://doi.org/10.5194/acp-8-5975-2008

Mahfouf, J. F. (2010). Assimilation of satellite-derived soil moisture from ASCAT in a limited-area NWP model. *Quarterly Journal of the Royal Meteorological Society: A journal of the atmospheric sciences, applied meteorology and physical oceanography*, *136*(648), 784–798.

Mohanty, U. C., Nayak, H. P., Sinha, P., Osuri, K. K., & Niyogi, D. (2019). Land surface processes over Indian summer monsoon region: A review. *Mausam*, *70*, 551–560.

Mohanty, U. C., Routray, A., Osuri, K. K., & Prasad, S. K. (2012). A study on simulation of heavy rainfall events over Indian region with ARW-3DVAR modeling system. *Pure and Applied Geophysics*, *169*(3), 381–399. https://doi.org/10.1007/s00024-011-0376-1

Nair, U. S., Rappin, E., Foshee, E., Smith, W., Pielke, R. A., Mahmood, R., et al. (2019). Influence of land cover and soil moisture based Brown Ocean effect on an extreme rainfall event from a Louisiana Gulf Coast tropical system. *Scientific Reports*, *9*(1), 1–10.

Namias, J. (1960). Factors in the initiation, perpetuation and termination of drought. *International Association of Scientific Hydrology Commission on Surface Waters Publication*, *51*, 81–94.

National Centers for Environmental Prediction/National Weather Service/NOAA/US Department of Commerce. (2000). NCEP FNL operational model global tropospheric analyses, continuing from July 1999. Research data archive at the National Center for Atmospheric Research, Computational and Information Systems Laboratory.

Nayak, H. P., Osuri, K. K., Sinha, P., Nadimpalli, R., Mohanty, U. C., Chen, F., et al. (2018). High-resolution gridded soil moisture and soil temperature datasets for the Indian monsoon region. *Scientific data*, *5*(1), 180264. https://doi.org/10.1038/sdata.2018.264

Niyogi, D. (2019). Land surface processes. In *Current trends in the representation of physical processes in weather and climate models* (pp. 349–370). Singapore: Springer. https://doi.org/10.1007/978-981-13-3396-5_17

Niyogi, D., Holt, T., Zhong, S., Pyle, P. C., & Basara, J. (2006). Urban and land surface effects on the 30 July 2003 mesoscale convective system event observed in the southern Great Plains. *Journal of Geophysical Research*, *111*, D19107. https://doi.org/10.1029/2005JD006746

Niyogi, D., Osuri, K. K., Subramanian, S., & Mohanty, U. C. (2016). The role of land surface processes on extreme weather events: Land data assimilation system. In *Advanced numerical modeling and data assimilation techniques for tropical cyclone prediction* (pp. 247–266). Dordrecht: Springer.

Osuri, K. K., Nadimpalli, R., Mohanty, U. C., Chen, F., Rajeevan, M., & Niyogi, D. (2017). Improved prediction of severe thunderstorms over the Indian monsoon region using high-resolution soil moisture and temperature initialization. *Scientific Reports*, *7*(1), 41377. https://doi.org/10.1038/srep41377

Pielke, R. A. Sr. (2001). Influence of the spatial distribution of vegetation and soils on the prediction of cumulus convective rainfall. *Reviews of Geophysics*, *39*(2), 151–177. https://doi.org/10.1029/1999RG000072

Pielke, R. A., Pitman, A., Niyogi, D., Mahmood, R., McAlpine, C., Hossain, F., et al. (2011). Land use/land cover changes and climate: modeling analysis and observational evidence. *Wiley Interdisciplinary Reviews: Climate Change*, *2*(6), 828–850. https://doi.org/10.1002/wcc.144

Prakash, S., Mitra, A. K., Momin, I. M., Rajagopal, E. N., Basu, S., Collins, M., et al. (2015). Seasonal intercomparison of observational rainfall datasets over India during the southwest monsoon season. *International Journal of Climatology*, *35*(9), 2326–2338. https://doi.org/10.1002/joc.4129

Rind, D. (1982). The influence of ground moisture conditions in North America on summer climate as modeled in the GISS GCM. *Monthly Weather Review*, *110*(10), 1487–1494. https://doi.org/10.1175/1520-0493(1982)110<1487:TIOGMC>2.0.CO;2

Rodell, M., Houser, P. R., Jambor, U. E. A., Gottschalck, J., Mitchell, K., Meng, C. J., et al. (2004). The global land data assimilation system. *Bulletin of the American Meteorological Society*, *85*(3), 381–394. https://doi.org/10.1175/BAMS-85-3-381

Routray, A., Mohanty, U. C., Niyogi, D., Rizvi, S. R. H., & Osuri, K. K. (2010). Simulation of heavy rainfall events over Indian monsoon region using WRF-3DVAR data assimilation system. *Meteorology and Atmospheric Physics*, *106*(1–2), 107–125. https://doi.org/10.1007/s00703-009-0054-3

Routray, A., Mohanty, U. C., Rizvi, S. R. H., Niyogi, D., Osuri, K. K., & Pradhan, D. (2010). Impact of Doppler weather radar data on numerical forecast of Indian monsoon depressions. *Quarterly Journal of the Royal Meteorological Society*, *136*(652), 1836–1850. https://doi.org/10.1002/qj.678

Saha, S., Moorthi, S., Wu, X., Wang, J., Nadiga, S., Tripp, P., et al. (2014). The NCEP Climate Forecast System Version 2. *Journal of Climate*, *27*(6), 2185–2208. https://doi.org/10.1175/JCLI-D-12-00823.1

Schär, C., Lüthi, D., Beyerle, U., & Heise, E. (1999). The soil-precipitation feedback: A process study with a regional climate model. *Journal of Climate*, *12*(3), 722–741. https://doi.org/10.1175/1520-0442(1999)012<0722:TSPFAP>2.0.CO;2

Sharma, K., Ashrit, R., Ebert, E., Mitra, A., Bhatla, R., Iyengar, G., & Rajagopal, E. N. (2019). Assessment of Met Office Unified Model (UM) quantitative precipitation forecasts during the Indian summer monsoon: Contiguous rain area (CRA) approach. *Journal of Earth System Science*, *128*(1), 4. https://doi.org/10.1007/s12040-018-1023-3

Shrivastava, S., Kar, S. C., & Sharma, A. R. (2017). Intraseasonal variability of summer monsoon rainfall and droughts over central India. *Pure and Applied Geophysics*, *174*(4), 1827–1844. https://doi.org/10.1007/s00024-017-1498-x

Shukla, J., & Mintz, Y. (1982). Influence of land-surface evapotranspiration on the Earth's climate. *Science*, *215*(4539), 1498–1501. https://doi.org/10.1126/science.215.4539.1498

Sikka, D. R. (1978). Some aspects of the life history, structure and movement of monsoon depressions. In *Monsoon Dynamics* (pp. 1501–1529). Basel: Birkhäuser. https://doi.org/10.1007/978-3-0348-5759-8_21

Taylor, C. M., Gounou, A., Guichard, F., Harris, P. P., Ellis, R. J., Couvreux, F., & De Kauwe, M. (2011). Frequency of Sahelian storm initiation enhanced over mesoscale soil-moisture patterns. *Nature Geoscience*, *4*(7), 430–433. https://doi.org/10.1038/ngeo1173

Trier, S. B., Chen, F., & Manning, K. W. (2004). A study of convection initiation in a mesoscale model using high-resolution land surface initial conditions. *Monthly weather review*, *132*(12), 2954–2976.

Tuttle, S., & Salvucci, G. (2016). Empirical evidence of contrasting soil moisture-precipitation feedbacks across the United States. *Science*, *352*(6287), 825–828.

Vaidya, S. S., Mukhopadhyay, P., Trivedi, D. K., Sanjay, J., & Singh, S. S. (2004). Prediction of tropical systems over Indian region using mesoscale model. *Meteorology and Atmospheric Physics*, *86*(1–2), 63–72. https://doi.org/10.1007/s00703-003-0019-x

Vinodkumar, A., Chandrasekar, A., Alapaty, K., & Niyogi, D. (2008). The impacts of indirect soil moisture assimilation and direct surface temperature and humidity assimilation on a mesoscale model simulation of an Indian monsoon depression. *Journal of Applied Meteorology and Climatology*, *47*(5), 1393–1412. https://doi.org/10.1175/2007JAMC1599.1

Vinodkumar, V., Chandrasekar, A., Alapaty, K., & Niyogi, D. (2009). Assessment of data assimilation approaches for the simulation of a monsoon depression over the Indian monsoon region. *Boundary-Layer Meteorology*, *133*(3), 343–366. https://doi.org/10.1007/s10546-009-9426-y

Xinmin, Z., Ming, Z., & Bingkai, S. (2000). A numerical study on effects of land—Surface heterogeneity from "combined approach" on atmospheric process Part II: Coupling—model simulations. *Advances in Atmospheric Sciences*, *17*(2), 241–255. https://doi.org/10.1007/s00376-000-0007-8

Yoon, J. H., & Huang, W. R. (2012). Indian monsoon depression: Climatology and variability. *Modern Climatology*, 45–72.

Zheng, Y., Kumar, A., & Niyogi, D. (2015). Impacts of land-atmosphere coupling on regional rainfall and convection. *Climate Dynamics*, *44*(9–10), 2383–2409. https://doi.org/10.1007/s00382-014-2442-8